SUBJECT: **SPIRE Spectrometer Pipeline Description**

PREPARED BY: **Trevor Fulton**

DOCUMENT No: **SPIRE-BSS-DOC-002966**

ISSUE: **Issue 4.0** **Date:** **18 January 2012**

APPROVED BY: **Date:**

Distribution

Name

Jean-Paul Baluteau	LAM
Trevor Fulton	Blue Sky Spectroscopy
Ed Polehampton	RAL
Peter Davis	Blue Sky Spectroscopy

Change Record

ISSUE	DATE	Changes
Draft 0.1	27 March 2007	First Version
Draft 0.2	02 May 2007	
Draft 0.3	09 May 2007	
Draft 0.4	27 June 2007	
Draft 0.5	10 July 2007	
Draft 0.6	31 August 2007	
Draft 0.7	26 September 2007	
Draft 0.8	02 October 2007	
Draft 0.9	10 April 2008	
Issue 1.0	23 May 2008	First Official Release
Issue 1.1	04 August 2008	Changed Section 2 to include a summary of the SPIRE Spectrometer AOTs.
		Changed Section 3 to describe the building block pipeline.
Issue 1.2	05 December 2008	Changes based on Phase One of the Science Validation Review [AD07]
Issue 1.3	30 April 2009	Changes based on Phase Two of the Science Validation Review [AD07, AD08]
Issue 2.0	18 October 2010	Updates to correspond to HCSS v5. • Removed Electrical and Optical Crosstalk correction steps. • Modified the description of the 1st level deglitching step. • Added a description to the temperature drift correction step. • Modified the default method of Baseline Correction. • Modified the default 2nd level deglitching algorithm for identification. • Added descriptions of the 2nd level glitch detection algorithms. • Changed order of steps in the "Modify Timelines" block. • Added descriptions for Instrument Correction, Telescope Correction. • Modified description for Phase Correction. • Modified the descriptions for extended and point-source flux conversion. • Added a description of the Level-2 product for Single pointing sparse sampling observations.
Issue 3.0	04 February 2011	Updates to correspond to HCSS v6. • Modified description for Phase Correction. • Moved Spectral Averaging to end of SOF1 pipeline. • Modified description for Spectral Averaging. • Removed Spectral Averaging from SOF2 pipeline.
Issue 4.0	18 January 2012	Updates to correspond to HCSS v7. • Swapped the order of Extended Flux Conversion and Telescope Correction. • Removed outlier rejection from Spectral Averaging. Updates to correspond to HCSS v8. • Spectral abscissa changed from Wavenumber (cm^{-1}) to Frequency (GHz). • Added sections for processing of observations in bright mode. o Added link to Section 2.1 of the SPIRE Pipeline Description document where PCAL processing is described. o Added Section 5 to describe steps specific to the bright mode pipelines.

TABLE OF CONTENTS

Glossary

ADC	Analog to Digital Converter
AOT	Astronomical Observation Template
BBID	Building Block Identifier
BSM	Beam Steering Mirror
FFT	Fast Fourier Transform
FT	Fourier Transform
FTS	Fourier Transform Spectrometer
HCSS	Herschel Common Science System
HIFI	Heterodyne Instrument for the Far Infrared
iFTS	Imaging Fourier Transform Spectrometer
ILS	Instrument Line Shape
IPAC	Infrared Processing and Analysis Center
JPL	Jet Propulsion Laboratory
LHS	Left Hand Side
LPF	Low Pass Filter
LVDT	Linear Variable Differential Transformer
MAD	Median Absolute Deviation
MPD	Mechanical Path Difference
NHKT	Nominal Housekeeping Timeline Product
OBSID	Observation Identifier
OPD	Optical Path Difference
PCAL	Photometer Calibrator
PFM	Proto-Flight Model
QCP	Quality Control Pipeline
RC	Resistor-Capacitor
RHS	Right Hand Side
RMS	Root Mean Square
RSRF	Relative Spectral Response Function
SBS	Spectrometer Beam Splitter
SCAL	Spectrometer Calibrator
SCR	Software Change Request
SDI	Spectrometer Detector Interferogram Product
SDS	Spectrometer Detector Spectrum Product
SDT	Spectrometer Detector Timeline Product
SLW	Spectrometer Long Wavelength
SMEC	SPIRE Spectrometer Mechanism
SMECT	Spectrometer Mechanism Timeline Product
SOF	Spectrometer Observation Format
SPG	Systematic Product Generation
SPIRE	Spectral and Photometric Imaging REceiver
SPP	SPIRE Pointing Product
SPR	Software Problem Report
SSO	Solar System Objects
SSW	Spectrometer Short Wavelength
SxR	Software Change Request or Software Problem Report
TBD	To Be Determined
TBW	To Be Written
WCS	World Coordinate System
WTMML	Wavelet Transform Modulus Maxima Lines
ZPD	Zero Path Difference

Symbols

Symbol	Description
$I(v)$	Vector of calibrated flux as a function of frequency
$I_i(v)$	Vector of calibrated flux as a function of frequency for a given detector, i
$I_{n\text{-}i}(v)$	Vector of calibrated flux as a function of time for a given detector, i, for a given mechanism scan, n
$I_{n\text{-}i}(v_k)$	The k^{th} calibrated flux sample for a given detector, i
$n(t)$	Vector of scan numbers as a function of time
$P(t)$	Vector of pointing positions as a function of time
$P_i(t)$	Vector of pointing positions as a function of time for a given detector, i
v	Regularly-sampled frequency vector
t	Regularly-sampled time vector
$V(t)$	Vector of voltages as a function of time
$V_i(t)$	Vector of voltages as a function of time for a given detector, i
$V_{n\text{-}i}(t)$	Vector of voltages as a function of time for a given detector, i, for a given mechanism scan, n
$V_{n\text{-}i}(t_k)$	The k^{th} voltage sample for a given detector, i
$V(v)$	Vector of voltages as a function of frequency
$V_i(v)$	Vector of voltages as a function of frequency for a given detector, i
$V(x)$	Vector of voltages as a function of optical path difference
$V_i(x)$	Vector of voltages as a function of optical path difference for a given detector, i
x	Regularly-sampled optical path difference vector
$z(t)$	Vector of spectrometer mechanism positions as a function of time

1. PURPOSE

The purpose of this document is to present an outline of the processing steps in the SPIRE spectrometer pipeline. The processing modules presented in this document follow those presented in Section 3 of AD01, which describes the steps that are common to both the SPIRE spectrometer and photometer pipelines.

1.1 Documents

1.1.1 Applicable Documents

Number	Document Name	Document Number	Issue
AD01	The SPIRE Analogue Signal Chain and Photometer Detector Data Processing Pipeline	SPIRE-UCF-DOC-002890	7
AD02	SPIRE Observers' Manual	HERSCHEL-HSC-DOC-0789	1.2
AD03	Operating Modes for the SPIRE Instrument	SPIRE-RAL-DOC-0000320	3.3
AD04	SPIRE FTS Mapping Modes	SPIRE-RAL-DOC-002801	1.0
AD05	SPIRE Pipeline Mask Policy	SPIRE-BSS-DOC-003127	1.4
AD06	SPIRE Pipeline Description	SPIRE-RAL-DOC-002437	2.1
AD07	FTS Pipeline Scientific Validation, Phase 1: Documentation Review Report		1.0
AD08	FTS Pipeline Scientific Validation: Documentation Review Responses		1.0

1.1.2 Reference Documents

Number	Description
RD01	Clipping Correction Task Performance, SPIRE-RAL-NOT-003270, Issue 1.0, August 2011
RD02	D. A. Naylor and M. K. Tahic, "Apodizing functions for Fourier transform spectroscopy," J. Opt. Soc. Am. A 24, 3644-3648 (2007)
RD03	Fulton, Trevor, “SPIRE Spectrometer Time Constant Derivation”, SPIRE-BSS-DOC-003204, Draft 0.2, 21 April 2009.
RD04	Fulton, Trevor, “Obliquity in the SPIRE Spectrometer”, SPIRE-BSS-DOC-000XXXX, Draft 0.3, 29 April 2008.
RD05	Davis, Peter, “Apodizing SPIRE Interferograms”, SPIRE-BSS-REP-003108, Draft 0.4, 29 May 2008.
RD06	SPIRE Sensitivity Models, SPIRE-QMW-NOT-000642, Issue 1.0, 21 May 2007.
RD07	Griffin, M.J. & Orton, G.S., "The Near Millimeter Brightness Temperature Spectra of Uranus and Neptune," Icarus, 105, 537, (1993).
RD08	R. V. Sudiwala, M. J. Griffin, & A. L. Woodcraft, “THERMAL MODELLING AND CHARACTERISATION OF SEMICONDUCTOR BOLOMETERS”, International Journal of Infrared and Millimeter Waves, Vol. 23, No. 4, April 200, p545

2. OVERVIEW

The data processing pipeline for the Spectral and Photometric Imaging Receiver (SPIRE) imaging Fourier Transform spectrometer (iFTS) contains processing modules commonly used to process FTS data, such as phase correction and the Fourier transform. The SPIRE iFTS pipeline also contains processing steps unique to SPIRE, such as the correction for the Herschel Telescope and Spectrometer Instrument.

The SPIRE iFTS pipeline has been designed to be consistent with the astronomical observation templates (AOTs) that are available to the users of the SPIRE spectrometer [AD03]. The final data products generated by the Spectrometer pipelines will in all cases consist of hyperspectral data; two spatial dimensions representing the astronomical region under study and one spectral dimension. The degree to which the hyperspectral data product is sampled both spatially and spectrally depends on the type of observation chosen.

2.1 Spatial Sampling

The spatial sampling in the final hyperspectral cubes depends on a combination of the number of requested raster pointing positions of the Herschel Telescope and the number of jiggle positions (the raster and jiggle patterns are defined in [AD04]) and of the SPIRE Beam Steering Mirror (BSM) selected. The number of Herschel Telescope pointing positions, n, will depend on the observing area requested and is limited by the maximum observing time for one observation (18 hours [AD02]). A list of the spatial sampling options available to astronomical observers is shown in Table 2.1.

Spatial Sampling	Astronomical Observation Template	Number of Herschel Telescope Raster Positions	Number of BSM Jiggle Positions	Total Number of Pointing Positions	Pixel Size [arcsec] SSW Band	Pixel Size [arcsec] SLW Band
Single, Sparse	SOF1	1	1	1	N/A	N/A
Single, Intermediate	SOF2	1	4	4	19.0	35.0
Single, Full	SOF2	1	16	16	9.5	17.5
Raster, Sparse	SOF1	n	1	n	38.0	70.0
Raster, Intermediate	SOF2	n	4	4n	19.0	35.0
Raster, Full	SOF2	n	16	16n	9.5	17.5

Table 2.1: SPIRE Spectrometer spatial sampling options [AD03]

2.2 Spectral Resolution

A SPIRE iFTS observation building block is defined as a set of equal-length scans of the SPIRE Spectrometer Mechanism (SMEC) at a single pointing position of the Herschel Telescope and SPIRE BSM. The spectral resolution of these scans is determined by the maximum optical path difference (OPD) that the instrument can achieve by displacing the SMEC from the point of symmetry, also known as the position of zero path difference (ZPD). The spectral resolution options available to astronomical observers for the SPIRE iFTS are shown in Table 2.2.

Spectral Resolution	Scan Length (OPD) [cm]	Spectral Resolution [GHz]	Spectral Resolution [cm^{-1}]
Low	0.60	24.98	0.83
Medium	2.08	7.207	0.240
High	12.56	1.193	0.0398

Table 2.2: SPIRE Spectrometer spectral sampling options

3. SPIRE SPECTROMETER BUILDING BLOCK PIPELINE

The block diagram of the SPIRE iFTS data processing pipeline is shown in Figure 3.1. The structure of the data processing pipeline specific to the SPIRE spectrometer follows the observation building blocks. This structure was chosen as it allows the processing modules that modify the signal data of the SPIRE spectrometer detectors to take advantage of symmetries and redundancies that are present for a series of FTS scans of the same astronomical target.

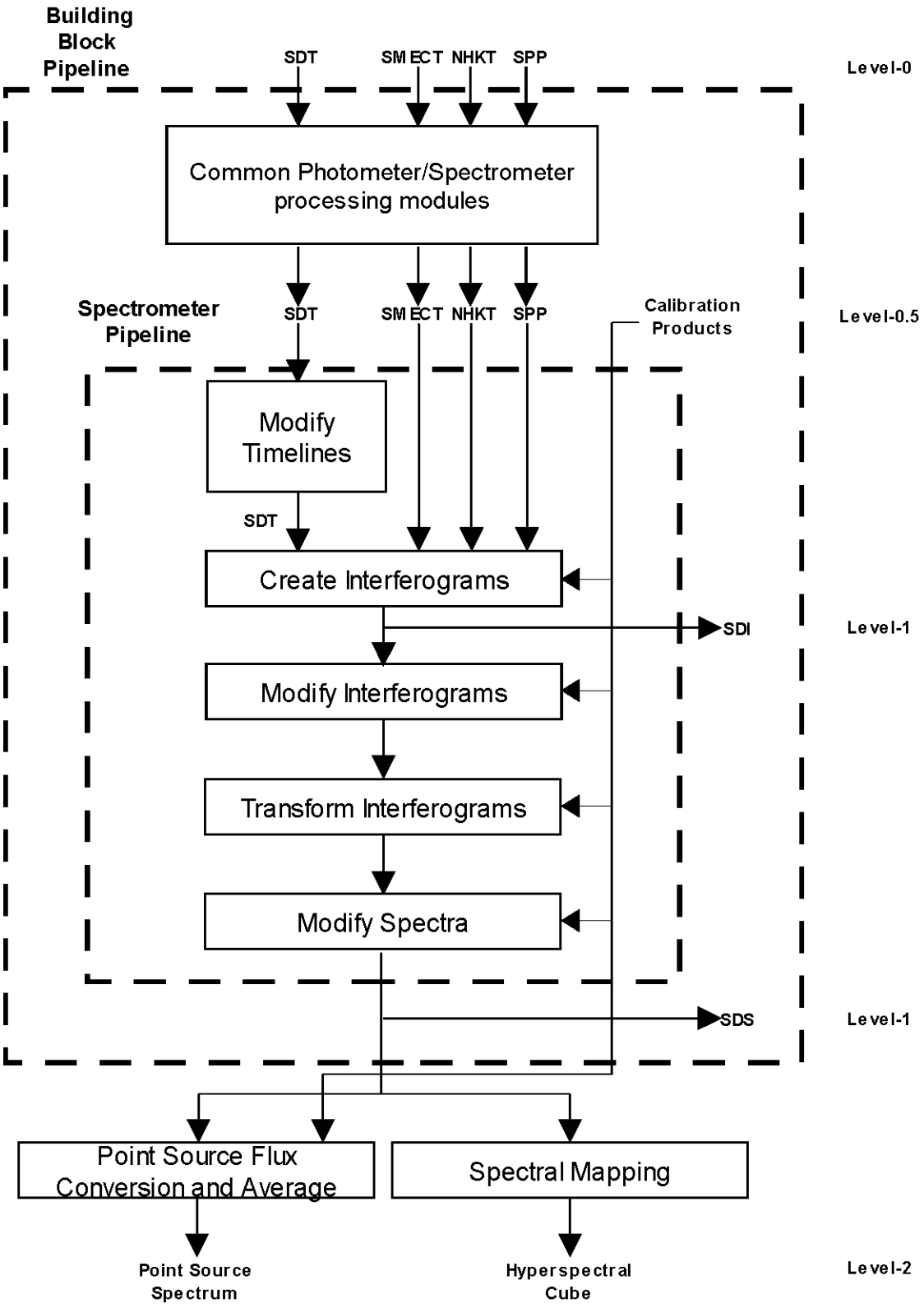

Figure 3.1: SPIRE iFTS data processing block diagram.

The data processing pipeline of the SPIRE spectrometer is split into two sections. The first of these sections (Section 3) describes the modules that make up the building block pipeline. The processing steps that combine the building block products are then described in Section 4. Section 5 describes the extra processing steps required when processing observations made with bright detector settings. The SPIRE spectrometer data processing pipeline described here operates on a single observation building block at a time. The building block pipeline consists of six major processing groups:

0. **Common Photometer/Spectrometer Processing modules.** The first steps of the SPIRE spectrometer and photometer pipelines are identical and are described in Section 3 of [AD01].
1. **Modify Timelines.** The processing modules in this group perform time domain operations on the spectrometer detector samples.
2. **Create Interferograms.** The processing modules in this group merge the timelines of the spectrometer detectors and spectrometer mechanism into interferograms. The spectrometer detector samples are split into different sets, with each set defined by a single scan of the spectrometer mechanism.
3. **Modify Interferograms.** The processing modules in this group perform operations on the spectrometer detector interferograms. These operations differ from those in the "Modify Timelines" group in that they are designed to act on spatial domain data rather than time domain data.
4. **Transform Interferograms.** The processing modules in this group transform the interferograms into a set of spectra.
5. **Modify Spectra.** The processing modules in this group perform operations on the spectrometer detector spectra.

3.1 Modify Timelines.

After application of the processing steps common to both the photometer and spectrometer detectors [Section 3 of AD01], the raw samples for each one of the 66 spectrometer detectors, labelled i, will have been converted into RMS voltage timelines, $V_{RMS\text{-}i}(t)$. These quantities are contained in the Level 0.5 Spectrometer Detector Timeline Product (SDT).

The processing modules described in the following sections are applied to the timelines for each spectrometer detector. Each of the processing steps contained in this processing block (see Figure 3.2) accepts a Level-0.5 SDT product as input and delivers an SDT product as output.

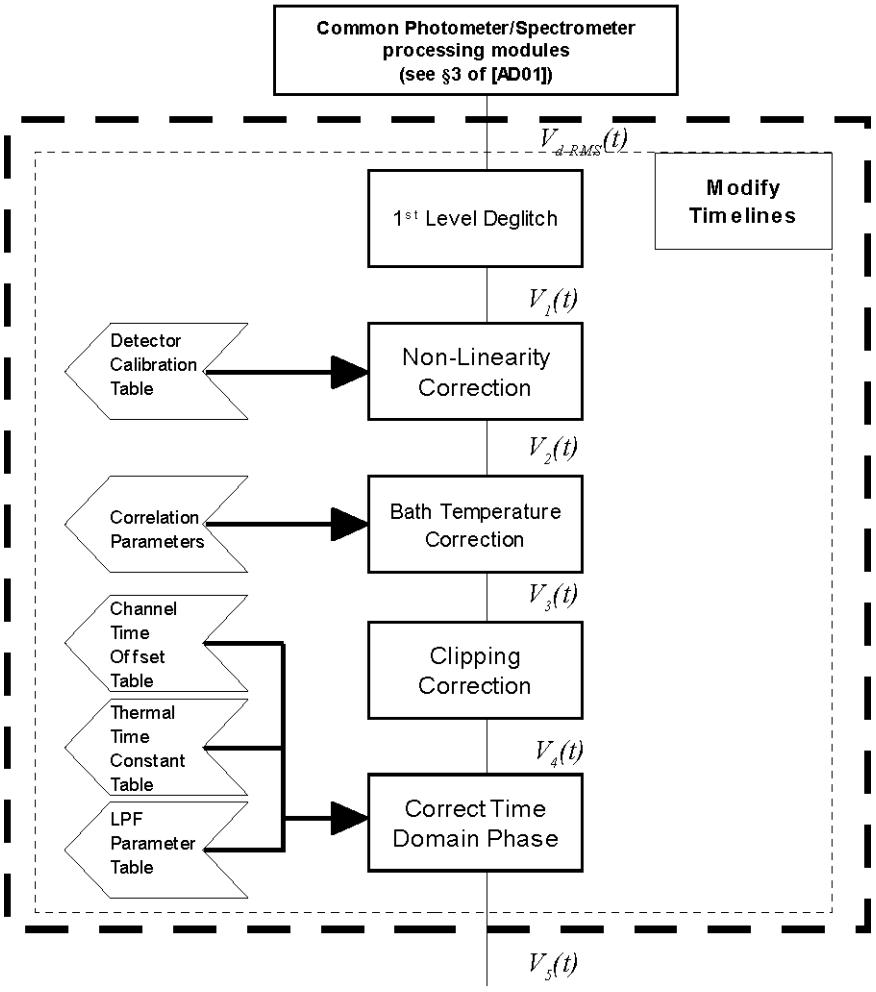

Figure 3.2: Modify Timelines portion of the SPIRE Spectromter building block pipeline.

3.1.1 First Level Deglitching

Glitches due to cosmic ray hits or other impulse-like events in the detectors will be removed using an algorithm based on a wavelet-based local regularity analysis (see Appendix A.1). This process is composed of two steps: the first step detects glitch signatures over the measured signal; the second step locally reconstructs a signal free of such glitch signatures.

1. **Glitch Identification.** Glitches are detected in the input SDT product by wavelet analysis assuming that the glitch signature is similar to the signature of a Dirac delta function. Each sample that is identified as a glitch will have its mask modified in accordance with the SPIRE pipeline mask policy [AD05].
2. **Glitch Reconstruction.** The samples identified as glitches are replaced by way of interpolation with a sixth-order polynomial.

The output of this module is the deglitched voltage timeline, $V_{1\text{-}i}(t)$ for detector i.

3.1.2 Detector Non-Linearity Correction

Even though bolometric detectors are commonly fabricated with highly linear response characteristics, the detectors of the SPIRE spectrometer will be subject to a wide dynamic range which makes a non-linear response likely. A dedicated non-linearity correction is designed to account for changes in the response of the detectors to strong signals. The form of this correction will be a function that is dependent on the amplitude of the signal itself as in Equation 3.1:

$$V_{2-i}(t) = \int_{V_0}^{V_{1-i}} \frac{f(V)}{f(V_r)} dV \tag{3.1}$$

where f(V), the real detector responsivity, V_r is a reference voltage, and V_0 is a fixed bolometer voltage. The normalized value of f(V) is derived as in Equation 3.2:

$$\frac{f(V)}{f(V_r)} = K_1 + \frac{K_2}{V - K_3} \tag{3.2}$$

A set of calibration tables, one per bias voltage, will each contain the values for V_0, K_1, K_2, and K_3 for each detector. Initially, the quantities in these calibration tables will be based on model predictions.

3.1.3 Removal of correlated noise due to bath temperature fluctuations

To first order, bath temperature fluctuations will influence all detectors in an array coherently – the temperature and corresponding output voltages will go up and down in synchronism. The bath temperature, T_0, may fluctuate due to temperature drifts within the instrument, and a set of timelines, $V_{th\text{-}i}(t)$, must be generated to correct for this. The most important effect of bath temperature variations for the level of fluctuations expected in SPIRE will be the direct response of the detector output voltage. Fluctuations in T_0 are expected to be much faster than a single, high-resolution scan of the spectrometer mechanism, so that this correction will be needed for such observations.

A correction timeline for each detector, $V_{th\text{-}i}(t)$, will be generated as follows:

1. The samples of the voltage timelines, V(t), of each of the thermistor and dark channels are binned to a width Δt=5 seconds.
2. A spline interpolation is then applied to the binned timelines to derive a smoothed timeline, $\underline{V_T}(t)$ for each of the thermistor and dark channels.
3. The correction timeline, $V_{th\text{-}i}(t)$, is then derived as in Equation 3.3:

$$V_{th-i}(t) = A \times \left(\underline{V_T}(t) - V_{T0}\right) + \frac{B}{2} \times \left(\underline{V_T}(t) - V_{T0}\right)^2, \tag{3.3}$$

   where the parameters A, B, and V_{T0} are all provided by a calibration product.

   Note: The module attempts to use the average of the two thermistor timelines for nominal detector mode and the average of the two dark channel timelines for bright detector mode to derive $\underline{V_T}(t)$. If either of these timelines is invalid, $\underline{V_T}(t)$ is derived from the remaining valid thermistor/dark channel timeline.
4. The input detector timelines, $V_{2\text{-}i}(t)$, are then corrected as in Equation 3.4:

$$V_{3-i}(t) = V_{2-i}(t) - V_{th-i}(t)\,. \tag{3.4}$$

3.1.4 Clipping Correction

The purpose of this processing step is to correct clipped signals in the input SDT product of the measured signals due to the limited range of the detector ADCs.

Clipped signals in the voltage timelines of the SDT are problematic as they are samples with incorrect values. The presence of clipped samples depends on the source strength and the detector offset setting. If left uncorrected, clipped samples can lead to further complications in particular when the timelines are converted into interferograms (Section 3.2.1).

Clipped samples can be corrected in a given SDT timeline using an eighth-order polynomial. While the only theoretical limit to the order of the polynomial is the total number of samples, the quality of its reconstruction has been found to depend on the number of clipped samples.

Ground based tests from the PFM4 test campaign have shown that a clipped signal of 40% of the theoretical peak (i.e. 60% of signal amplitude is left over) corresponds to four clipped samples (at ZPD) and to eight clipped samples (for secondary peaks) per scan. In this case, the restored signal has an RMS error of 2%-3% of signal amplitude at ZPD. That corresponds to less than 1% RMS error on the final reconstructed spectrum continuum. The same tests showed that a clipped signal that results in an 80% reduction of the ZPD amplitude results in an RMS error of up to 6% on the reconstructed interferogram signal.

The process by which clipped timelines are corrected is described below.

1. **Identify the clipped samples in the SDT timelines.** Let $V_{3\text{-}i}(t_k)$ denote those samples that have been flagged as being clipped, let $V_{3\text{-}i}(t_j)$ represent all other samples, and let i represent a given spectrometer detector.
2. **Interpolate the modified SDT timeline.** A polynomial of degree eight (8) is applied to the five points before and after those identified as being clipped.
3. **Replace the SDT timeline.** Replace those samples that had been identified as clipped in the original detector timeline, $V_{3\text{-}i}(t_k)$, with the results of the polynomial fit, $V_{fit}(t_k)$.
$$V_{4-i}(t_k) = V_{fit}(t_k) \tag{3.5}$$
4. **Identify the corrected samples in the SDT timelines.** Samples that have been corrected, as in Equation 3.5, should be flagged as having been corrected.
5. **Propagate the remainder of the SDT timelines.** Samples that were not identified as being clipped, $V_{3\text{-}i}(t_j)$ are simply propagated to the resultant timeline, $V_{4\text{-}i}(t)$.
$$V_{4-i}(t_j) = V_{3-i}(t_j) \tag{3.6}$$

Tests of the clipping correction show that even in cases where the interferogram was clipped such that the fourth lobe away from zero path difference was affected, the spectrum could be corrected to better than 3%. When up to three consecutive points were clipped at ZPD for SSW and up to five consecutive points for SLW, the effect on the final spectrum was much less than 1% [RD01].

3.1.5 Time Domain Phase Correction

The purpose of the Time Domain Phase Correction module is to correct the detector timelines, $V_{4\text{-}i}(t)$, for delays induced by the filters in the readout electronics and the thermal response of the detectors themselves.

3.1.5.1 Determination of the Induced Phase Shift

The SPIRE spectrometer detector chain contains a 6-pole Bessel low pass filter (LPF) as well as an additional RC LPF (see Section 3.5 of AD01) The transfer function of which is shown in Equation 3.7,

$$H_{LPF}(\omega) = \left[\frac{2.87}{1+7.85\times10^{-3}(j\omega)+16.03\times10^{-6}(j\omega)^2}\right]\times \left[\frac{1}{1+3.23\times10^{-3}(j\omega)+400\times10^{-6}(j\omega)^2}\right]\times \left[\frac{1}{1+6.26\times10^{-3}(j\omega)+14.65\times10^{-6}(j\omega)^2}\right]\times\left[\frac{1}{1+1\times10^{-4}(j\omega)}\right] \quad (3.7)$$

where $\omega=2\pi f$ and f is the frequency of the recorded signal.

In addition to the response due to the electronic LPFs, the thermal response of the SPIRE bolometers needs to be taken into account. As was shown in Section 4 of AD01, the frequency response of the SPIRE bolometers may be modelled as a combination of a fast and a slow detector-specific time constant -- τ_1 and τ_2, respectively. The overall thermal response thus takes the form shown in Equation 3.8,

$$H_{Bol}(\omega) = \frac{1-a_i}{1+j\omega\tau_{1-i}} + \frac{a_i}{1+j\omega\tau_{2-i}}. \quad (3.8)$$

These two effects may be combined into a single detector transfer function, given by Equation 3.9:

$$H_{LPF}(\omega) = \left[\frac{2.87}{1+7.85\times10^{-3}(j\omega)+16.03\times10^{-6}(j\omega)^2}\right]\times \left[\frac{1}{1+3.23\times10^{-3}(j\omega)+400\times10^{-6}(j\omega)^2}\right]\times \left[\frac{1}{1+6.26\times10^{-3}(j\omega)+14.65\times10^{-6}(j\omega)^2}\right]\times\left[\frac{1}{1+1\times10^{-4}(j\omega)}\right]\times\left[\frac{1-a_i}{1+j\omega\tau_{1-i}}+\frac{a_i}{1+j\omega\tau_{2-i}}\right] \quad (3.9)$$

Note: Ground-based studies of the thermal response of the SPIRE spectrometer detectors suggest that the fast time constant by itself sufficiently characterizes their behaviour [RD03] (i.e. $a_i=0$, $\tau_2=0$). Nevertheless, this aspect will be monitored over the course of the mission. In addition, it is not anticipated that the fast time constant will depend on detector bias voltage, though this behaviour will likewise be monitored over the course of the mission.

The combined response of the electronic LPFs and the thermal behaviour of the SPIRE bolometer detectors, $H_{TOTAL}(\omega)$, will affect both the magnitude (Equation 3.10) and the phase (Equation 3.11) of the signals recorded by the SPIRE detectors.

$$\text{Magnitude}(H_{TOTAL-i}(\omega)) = \left|H_{TOTAL-i}(\omega)\right|. \quad (3.10)$$

$$\text{Phase}(H_{TOTAL-i}(\omega)) = \phi_{TOTAL-i}(\omega) = \text{Tan}^{-1}\left|\frac{\text{Im}(H_{TOTAL-i}(\omega))}{\text{Re}(H_{TOTAL-i}(\omega))}\right|. \quad (3.11)$$

According to Fourier theory, a change of phase in the spectral domain corresponds to a time shift in the temporal domain. This effect is particularly problematic for the SPIRE spectrometer in scanning mode (SOF1 and SOF2 [AD03]), where the delay induced by the electronic and thermal phase can lead to errors in the interpolation of the detector signals (see Section 3.2.1).

The time domain phase correction function, TDPCF, is quantified as the inverse Fourier Transform of the frequency domain phase shift as in Equation 3.12,

$$\mathrm{TDPCF}_i(t) = FT^{-1}\left[e^{-i\phi_{TOTAL-i}(\omega)}\right]. \quad (3.12)$$

3.1.5.2 Correction of the Induced Shift

The input timelines ($V_{4\text{-}i}$) are corrected by way of time convolution with the TDPCF(t), resulting in a set of corrected timelines, $V_{5\text{-}i}$

$$V_{5-i}(t) = V_{4-i}(t) \otimes \mathrm{TDPCF}_i(t). \quad (3.13)$$

3.2 Create Interferograms

The pipeline modules listed to this point describe the operations that will be performed on the detector timelines in the Level 0.5 SDT product. At this point, in the SPIRE iFTS building block pipeline, three additional Level 0.5 products are required to proceed: the Spectrometer Mechanism Timeline product (SMECT); the Nominal Housekeeping Timeline product (NHKT); and the SPIRE Pointing product (SPP) (see Figure 3.3).

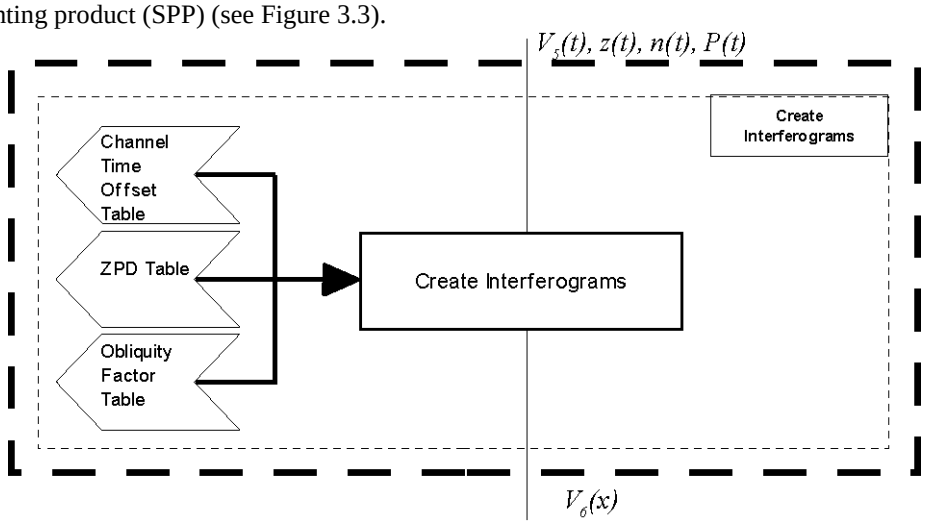

Figure 3.3: Interferogram creation block of the SPIRE Spectrometer pipeline

3.2.1 Interferogram Creation

A single building block of a SPIRE spectrometer observation in scanning mode consists of a series of scans of the spectrometer mechanism while the instrument is pointed at a given target. The sampling of the SPIRE spectrometer detectors and the spectrometer mechanism is decoupled; the two subsystems are sampled at different rates and at different times. In order to derive the source spectrum from the measured data, the spectrometer detector samples must be linked with the position of the SMEC in the form of interferograms. Additionally, the SMEC positions onto which the spectrometer detector signal samples are to be interpolated should be regularly spaced in terms of optical path difference (OPD).

The process by which interferograms are created involves two steps, each of which is described below.

1. **Interpolation of the SMEC timeline.** This step converts the spectrometer mechanism timeline from one that is non-uniform in position to one that is uniform in position.
    a. **Establish a common OPD position vector.** This step creates a common vector of OPD positions that will be the basis of the interferograms for all of the spectrometer detectors and for all of the scans in the observation. This common position vector will contain samples that are uniformly-spaced in terms of OPD position as well as a sample at the position of zero-path-difference (ZPD).

       The step size of the common OPD vector is chosen in such a way as to match the sampling rate of the spectrometer detector signal samples. For an SDT sampling rate s [Hz] and a SMEC scanning speed v_{SMEC} [cm/s MPD], the position step size, ΔMPD in units of cm; is given by:

$$\Delta\mathrm{MPD} = v_{SMEC} / s. \quad (3.14)$$

       This step is then converted such that it is in terms of OPD by the following relation

$$\Delta\mathrm{OPD} = \mathrm{FLOOR}\left[4\Delta\mathrm{MPD}\right]. \quad (3.15)$$

where FLOOR[] denotes that the step size is rounded down to the nearest integer in units of μm OPD and the factor of four is the nominal conversion between MPD and OPD for a Mach-Zehnder FTS. Using the nominal SPIRE spectrometer settings — s=80Hz, vSMEC=0.05cm/s — this results in an OPD step size of 25 μm.

b. **Map the common OPD position vector to a SMEC position vector for each spectrometer detector.** This step maps, for each spectrometer detector, the common OPD positions established in the preceding positions in units of mechanical path difference. This step involves: a scaling factor, f [RD04], which takes into account the obliquity in the SPIRE FTS; and a shift, ZPD, which establishes the position of zero optical path difference. Since these quantities are unique to each spectrometer detector, i, this mapping is performed on a detector-by-detector basis and is shown in Equation 3.16.

$$\mathrm{MPD}_i = \frac{\mathrm{OPD}}{f_i} + \mathrm{ZPD}_i. \quad (3.16)$$

c. **Parse the measured SMEC timeline into discrete scans.** This step splits the full SMEC timeline ($z(t_{SMEC})$) from the input SMECT product into a series of discrete timelines, $z_n(t_{SMEC})$. Each of the discrete timelines, $z_n(t_{SMEC})$, represents one spectrometer scan. The delineation of the SMEC timeline is accomplished by comparing consecutive SMEC position samples and finding those samples where the motion of the mirror mechanism changed direction.

d. **Interpolate the measured SMEC timelines onto the mapped SMEC timelines.** The next step is to determine, on a detector-by-detector and scan-by-scan basis, the times when the spectrometer mechanism reached the mapped SMEC positions. Since, for each detector, there is a 1:1 relationship between the mapped SMEC positions and the regularly spaced OPD positions, this step effectively determines the times when the SMEC reached the regularly spaced OPD positions for each detector

$$z_n(t_{SMEC}) \rightarrow \mathrm{MPD}_{n-i}(\mathrm{t}_{\mathrm{MPD}_i}). \quad (3.17)$$

2. **Merge the spectrometer detector and the mapped SMEC timelines.** This step combines the signal samples from the signal timeline of a given spectrometer detector ($V_{6\text{-}i}(t_i)$) with the mapped SMEC timelines.

a. **Interpolation of the spectrometer detector timelines.** The input spectrometer detector signal samples, $V_{6\text{-}n\text{-}i}(t_i)$, are mapped onto the times corresponding to the regular MPD ($t_{MPD\text{-}i}$) positions by way of interpolation. Since there is a 1:1 relationship between these time samples, $t_{MPD\text{-}i}$, and the regular MPD positions, MPD_i, this interpolation effectively maps, for each detector, the signal samples to the regularly spaced MPD positions. Moreover, since there is a 1:1 relationship between the regular MPD positions for each detector and the common OPD positions (as shown in Equation 3.16), this step accomplishes the mapping of the signal samples for each detector to the common OPD positions, which is the resultant interferogram that is desired, $V_{6\text{-}n\text{-}i}(OPD)$

$$V_{5-n-i}(t_i) \rightarrow V_{5-n-i}(\mathrm{t}_{\mathrm{MPD}\text{-}i}) \rightarrow V_{5-n-i}(\mathrm{t}_{\mathrm{OPD}}) \rightarrow V_{5-n-i}(\mathrm{OPD}) \equiv V_{6-n-i}(x), \quad (3.18)$$

where n and i in Equation 3.18 refer to the SPIRE Mechanism scan number and the SPIRE Spectrometer detector number, respectively.

Note: Signal samples flagged as having been clipped at the OPD extrema are excluded from the resultant interferograms.

b. **Affix a pointing value to the resultant interferogram.** Upon creation of each interferogram, $V_{6\text{-}n\text{-}i}(x)$, the pointing timeline for each detector i, $P_i(t)$ is evaluated and its time-averaged value is affixed to each spectrometer detector for each interferogram in the building block.

3.3 Modify Interferograms

The pipeline modules described in this section perform operations on the interferograms created in the previous step. Each of the processing steps contained in this processing block accepts an SDI product as input and delivers an SDI product as output (see Figure 3.4).

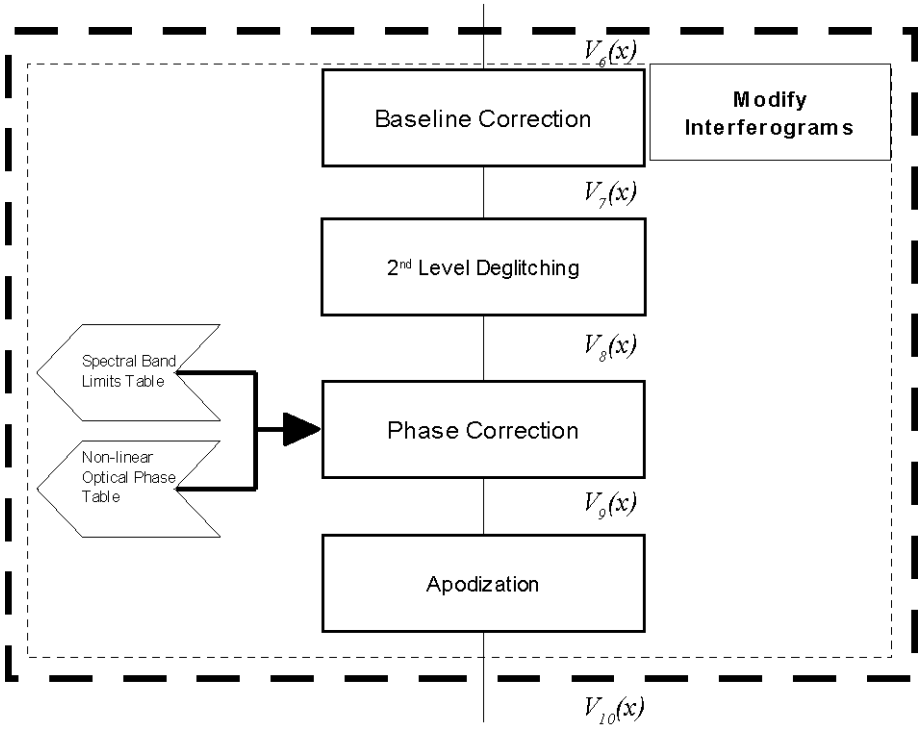

Figure 3.4: Interferogram modification block of the SPIRE Spectrometer pipeline.

3.3.1 Interferogram Baseline Correction

According to the equations presented in Appendix A.2, the overall intensity incident on the SPIRE spectrometer detectors can be separated into two components: an offset or baseline portion that is a function of OPD; and a component that is modulated as a function of OPD. On a detector-by-detector and scan-by-scan basis, the baseline correction algorithm evaluates and removes the baseline portion of the derived interferogram ($V_{7\text{-}i}(x)$). The baseline correction processing step provides two methods to evaluate the baseline of the derived interferograms: fitting by way of the Fourier transform (default); and polynomial fitting.

1. **Fourier transform fitting.** The interferogram baseline is evaluated as that portion of the measured interferograms whose Fourier components are at frequencies lower than 119.916 GHz (4 cm^{-1}) (Equation 3.19).

$$V_{Baseline-i}(x) = FT^{-1}\left[FT\left[V_{6-i}(x)\right]_{V=4}^{V=0}\right]. \quad (3.19)$$

2. **Polynomial fitting.** The interferogram baseline evaluated by way of a using a fourth-order polynomial (Equation 3.20).

$$V_{Baselinee-i}(x) = a_i + b_i x + c_i x^2 + d_i x^3 + e_i x^4 . \quad (3.20)$$

Both the Fourier transform and polynomial and fitting methods will disregard those samples at OPD extrema that have been identified as having been clipped.

Regardless of the method used to determine the interferogram baseline, once evaluated, this baseline is removed from the measured interferogram by subtraction

$$V_{7-i}(x) = V_{6-i}(x) - V_{Baseline-i}(x). \quad (3.21)$$

In the Interactive processing mode, this module will provide an option to return not only the corrected Interferogram product, $V_{7\text{-}i}(x)$, but also a product that contains the fitted interferogram baselines, $V_{Baseline\text{-}i}(x)$.

Note: The nominal method of interferogram baseline evaluation that will be employed by this processing module will be the Fourier transform fitting method. This method was chosen as the interferogram baseline fluctuations observed in flight data, in particular for strong sources, are not well-defined by a low order polynomial.

3.3.2 Second Level Deglitching

Localized artefacts in the interferograms, glitches, pose a serious problem for Fourier Transform Spectrometer observations. As such, a glitch that affects as few as one interferogram sample can adversely affect each and every spectral component. Glitches in an interferogram must therefore be identified and removed prior to transformation in order to avoid unwanted spectral artefacts.

Glitch Identification. Glitches are identified for each spectrometer detector, i, by comparing, on a OPD position-by-OPD position basis (i.e. each x_k), the samples from one scan, j, to those from all other scans in the same observation building block derived from the same mechanism scan direction (scan number n, where $n \neq j$ and all n and j are from the same mechanism scan direction). The samples that deviate more than a prescribed amount from the median are flagged as glitches and will have their sample masks modified in accordance with the SPIRE pipeline mask policy [AD05].

Based on in-flight data, the most effective statistical metric found for identifying second-level glitches is the median absolute deviation (MAD) algorithm (all four glitch detection algorithms are described in Appendix A.5). This algorithm first computes, for a given detector and SMEC scan direction, the median signal and median absolute deviation at each OPD position from all of the measured interferograms. A given OPD position, x_k, is considered to contain a glitch if its signal value differs from the median signal value at that position by more than a threshold, *d*:

$$\left|V_{7-i}(x_k) - MEDIAN\left(V_7(x_k)\right)\right| > d \tag{3.22}$$

The threshold, *d*, in Equation 3.22 is determined dynamically based on the number of scans, n, in the input data product such that the module would consider valid data as an outlier **0.1%** of the time. See Appendix A.4 for further explanation.

Glitch Correction. The samples that are identified as glitches are then replaced. For a glitch at a given position for a given spectrometer detector, the value of the replacement sample is determined by the average of the non-glitch samples from the other observed interferograms at that position. Each sample that is replaced will have its sample mask modified in accordance with the SPIRE pipeline mask policy [AD05]

$$V_{j-8-i}(x_k) = \frac{1}{N_{Scans} - 1} \sum_{n=1, n\neq j}^{N_{Scans}} V_{n-7-i}(x_k)\,. \tag{3.23}$$

Note: The two steps of the interferogram deglitching module rely on a statistical analysis of the measured interferograms. Those observations that contain the minimum allowed number of four interferograms (two per scan direction) per observation building block [AD02] could potentially pose a problem with this method. In this situation, this processing step uses all four interferograms per detector so that these statistics are meaningful.

3.3.3 Phase Correction

The symmetry of a Fourier Transform spectrometer theoretically implies that interferograms recorded by the spectrometer will exhibit even symmetry. Since the spectrum of an evenly symmetric interferogram contains only real components, it is therefore expected that the phase should be zero for all spectral components.

The presence of dispersive elements and the possibility that the position of zero path difference not being sampled can, however, result in an interferogram whose signal samples are not symmetric about ZPD. In this scenario, the phase that is expected would take the form shown in Equation 3.24:

$$\phi_{\exp-i}(\nu) = \phi_{\mathrm{NonLin}-i}(\nu) + \phi_{\mathrm{Random}-i}(\nu)\,, \tag{3.24}$$

where the $\varphi_{\mathrm{NonLin\text{-}i}}(\nu)$ term is a non-linear phase that represents the effects of the dispersive elements is derived from calibration measurements for each detector and each SMEC scan direction, and $\varphi_{\mathrm{Random\text{-}i}}(\nu)$ represents any phase due to noise.

The non-linear phase term is derived per scan direction on a detector-by-detector basis from the phase of all the low-resolution portions of the average interferogram for the observation. The non-linear phase term is removed from the measured interferograms in the spectral domain as follows:

1. **Transform to the spectral domain.** The Fourier transform is applied to both the measured interferograms, $V_{8\text{-}n\text{-}i}(x)$, and the average interferograms, $\overline{V_{8-n-i}(x_{LR})}$. In order to ensure that the spectral sampling intervals of the transformed interferogram and the calibrated phase are the same, zero-padding (see Section 3.4.1) is applied prior to transformation.

$$V_{8-n-i}(\nu) = FT\left[V_{8-n-i}(x)\right] \tag{3.25}$$

$$\overline{V_{8-n-i}(\nu)} = FT\left[\overline{V_{8-n-i}(x_{LR})}\right]. \tag{3.26}$$

2. **Derive the non-linear phase.** The $\varphi_{\text{NonLin-i}}(\nu)$ term is derived as in Equation 3.27,

$$\phi_{NonLin-i}(\nu) = \text{Tan}^{-1}\left[\frac{\text{Im}\left(\overline{V_{8-n-i}(\nu)}\right)}{\text{Re}\left(\overline{V_{8-n-i}(\nu)}\right)}\right]. \tag{3.27}$$

3. **Correct the transformed interferogram.** A common spectral sampling interval having been ensured, the spectrum of the measured interferogram is corrected by way of multiplication with the calibrated phase,

$$V_{9-n-i}(\nu) = V_{8-n-i}(\nu) \times e^{-i\phi_{Cal}(\nu)} \tag{3.28}$$

4. **Apply the inverse transform to the corrected spectrum.** The inverse Fourier transform is applied to the corrected spectrum, $V_{9\text{-}n\text{-}i}(\nu)$, to create the corrected interferogram, $V_{9\text{-}n\text{-}i}(x)$,

$$V_{9-n-i}(x) = IFFT\left[V_{9-n-i}(\nu)\right] \tag{3.29}$$

and the zeros added in the first step are removed.

Note: Throughout the mission, the efficacy of the calibrated non-linear phase curves will be monitored. If observations exhibit a significant residual phase after the processing step, if may be necessary to derive and apply a specialized calibration product in this step.

3.3.4 Apodization

The natural instrument line shape (ILS) for a Fourier Transform spectrometer is a cardinal sine, or Sinc function. If the source signal contains features at or near the resolution of the spectrometer, the ILS can introduce secondary maxima in the spectra. The apodization functions available within this module may be used to reduce these secondary maxima at the cost of reducing the resolution of the resultant spectrum. The apodization module in the SPIRE spectrometer data processing pipeline offers a number of apodizing functions to allow for an optimal trade-off between reduction in the secondary maxima and reduced resolution [RD02, RD05].

Apodization is performed by multiplying the input interferograms ($V_{\text{n-9-i}}(x)$), on a detector-by-detector and on a scan-by-scan basis with a tapering or apodizing function.

$$V_{10-i}(x) = V_{9-i}(x) \times \text{Apod}(x). \tag{3.30}$$

A list of the available apodization functions, their keyword abbreviations, and the mathematical operations they perform on interferometric data is given in Table 3.1. Also shown in Table 3.1 is the default apodization function that is to be used for Standard Product Generation.

Apodization Function	Keyword	Formula
HANNING	aHN_17	$0.50 + 0.50\cos(\pi x)$
HAMMING	aHM_15	$0.54 + 0.46\cos(\pi x)$
Gaussian	aGauss_19	$\exp(-x^2/2\sigma^2)$, $\sigma^2 = -0.5/\ln(0.01)$
Norton-Beer 1.1	aNB_11	$0.701551 - 0.639244\,(1-x^2) + 0.937693\,(1-x^2)^2$
Norton-Beer 1.2	aNB_12	$0.396430 - 0.150902\,(1-x^2) + 0.754472\,(1-x^2)^2$
Norton-Beer 1.3	aNB_13	$0.237413 - 0.065285\,(1-x^2) + 0.827872\,(1-x^2)^2$
Norton-Beer 1.4	aNB_14	$0.153945 - 0.141765\,(1-x^2) + 0.987820\,(1-x^2)^2$
Norton-Beer 1.5	**aNB_15**	$\mathbf{0.077112 + 0.703371\,(1-x^2)^2 + 0.219517\,(1-x^2)^4}$
Norton-Beer 1.6	aNB_16	$0.039234 + 0.630268\,(1-x^2)^2 + 0.234934\,(1-x^2)^4 + 0.095563\,(1-x^2)^6$
Norton-Beer 1.7	aNB_17	$0.02007835 + 0.4806674\,(1-x^2)^2 + 0.386409\,(1-x^2)^4 + 0.1128451(1-x^2)^6$
Norton-Beer 1.8	aNB_18	$0.01017233 + 0.3444297\,(1-x^2)^2 + 0.451817\,(1-x^2)^4 + 0.1935809(1-x^2)^6$
Norton-Beer 1.9	aNB_19	$0.004773004 + 0.2324736\,(1-x^2)^2 + 0.4645618\,(1-x^2)^4 + 0.2981915(1-x^2)^6$
Norton-Beer 2.0	aNB_20	$0.002267285 + 0.1404125\,(1-x^2)^2 + 0.4871719\,(1-x^2)^4 + 0.2562002(1-x^2)^6 + 0.1139479\,(1-x^2)^8$

Table 3.1: Apodization functions available within SPIRE pipeline processing. The default apodization function, Norton Beer 1.5, is highlighted. Each formula shown is normalized to an interferogram of unit length.

The baseline approach for Standard Product Generation will be to provide two spectral products per observation building block: one in which the default apodization function has been applied to the recorded interferograms; the other where no apodization has been applied.

3.4 Transform Interferograms

At this point in the building block pipeline, the operations that are best performed in the interferogram domain have been implemented. From this point on, further processing can take place in the spectral domain. As such, this presents the opportunity to transform the interferograms for each detector, $V_{n\text{-}i}(x)$, to the spectral domain. The section describes the process by which the interferograms contained in the Level 1 SDI product created by the preceding steps are transformed to spectra that will be contained in a Level 1 Spectrometer Detector Spectrum (SDS) product (see Figure 3.5).

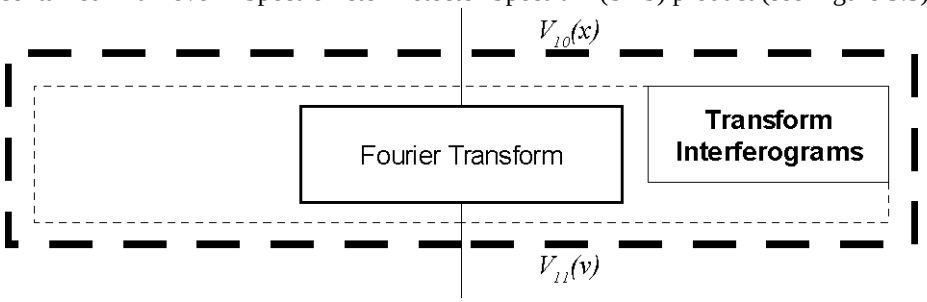

Figure 3.5: Interferogram transformation block of the SPIRE Spectrometer pipeline

3.4.1 Fourier Transform

The purpose of the Fourier Transform module is to transform the set of interferograms from a SPIRE spectrometer observation into a set of spectra. This processing module is capable of transforming both double-sided and single-sided interferograms (see Appendix A.3 for the definition of double-sided and single-sided interferograms).

Both the double-sided transform and the single-sided transform are applied to data from the SPIRE FTS *regardless of the spectral resolution mode*. The double-sided transform is applied before phase correction (Section 3.3.3) so that the phase may be evaluated. The single-sided transform is applied after apodization (Section 3.3.4) -- when all of the asymmetric components of the interferograms have been removed.

Double-sided Transform. For the double-sided transform, each interferogram in the SDI is examined and only the double-sided portion of the interferogram is used to compute the resultant spectrum. The resultant spectra will contain both real and imaginary components.

$$V_{11-i}(\nu) = FT\left[V_{10-i}(x)\,|_{-L}^{L}\right] = \int_{-L}^{L} V_{10-i}(x) e^{-i2\pi\nu x} dx \tag{3.31}$$

In this case, the discrete Fourier transform that is used to compute the spectral components takes the form shown in Equation 3.32.

$$V_{11-i}(\nu_k) = \sum_{n=0}^{N} V_{10-i}(x_n) e^{-i\frac{2\pi mk}{N}} \tag{3.32}$$

Single-sided Transform. In the case of the single-sided transform, only those interferogram samples to one side of the position of zero path difference are considered. The spectra that result from the single-sided transform therefore contain only real components.

$$V_{11-i}(\nu) = FT\left[V_{10-i}(x)\,|_{0}^{L}\right] = \int_{0}^{L} V_{10-i}(x)\cos(2\pi\nu x) dx \tag{3.33}$$

The discrete Fourier transform that is used to compute the spectral components for single-sided interferograms takes the form shown in Equation 3.39.

$$V_{11-i}(\nu_k) = \sum_{n=0}^{N} V_{10-i}(x_n) \cos\left(\frac{2\pi nk}{N}\right) \tag{3.34}$$

Frequency Grid. For both the single-sided and double-sided transforms the frequency grid onto which the spectrum is registered is calculated based on the interferogram sampling rate (ΔOPD) and on the maximum OPD displacement from the position of ZPD, L.

The Nyquist frequency (ν_{Nyquist}), the maximum independent frequency in the output spectrum, is given by:

$$\nu_{Nyquist} = \frac{1}{2\Delta\mathrm{OPD}} \times 10^{-7} c \tag{3.35}$$

The spacing between independent spectral samples ($\Delta\nu$) is given by

$$\Delta\nu = \frac{1}{2L} \times 10^{-7} c \tag{3.36}$$

The spacing between spectral samples can be modified by padding the interferogram with zeroes. This procedure does not add any information to the spectrum but allows for an easier comparison between observations. In this case, a zero-padded interferogram ($V_{12\text{-}ZP\text{-}i}$) is given by

$$V_{11-ZP-i}(x) = V_{10-i}(x)\,|_0^L, 0\,|^{L<x\le L_{ZP}} \tag{3.37}$$

The corresponding spectral sampling interval is given by

$$\Delta\nu_{ZP} = \frac{1}{2L_{ZP}} \times 10^{-7} c\,. \tag{3.38}$$

The resultant spectrum of the zero-padded interferogram is given by

$$V_{11-ZP-i}(\nu_k) = \sum_{n=0}^{N_{ZP}} V_{10-ZP-i}(x_n) \cos\left(\frac{2\pi nk}{N_{ZP}}\right) \tag{3.39}$$

The scan lengths and resultant spectral sampling intervals for the three distinct spectral resolutions from Section 6.6 of AD02 are given in Table 3.2.

Spectral Resolution [AD02]	Sampling Interval (OPD) [μm]	Nyquist Frequency [GHz]	Padded Scan Length (OPD) [cm]	Spectral Sampling Interval [GHz]
Low	25	5995.85	2.0	7.495
Medium	25	5995.85	10.0	1.499
High	25	5995.85	50.0	0.299

Table 3.2: Interferogram Padding

Spectral Normalization.
The final step of the Fourier Transform processing task is to normalize the calculated spectra to unit frequency. This is accomplished by dividing each spectral element, $V_{12\text{-}i}(\nu_k)$, by the spectral sampling interval, $\Delta\nu$

$$V_{11-i}(\nu_k) = \frac{V_{11-i}(\nu_k)}{\Delta\nu}\,. \tag{3.40}$$

3.5 Modify Spectra

The pipeline modules that follow in this section describe the operations that will be performed on the Level-0.5 SDS products that were created in the preceding step. The end result of these spectral modifying processing steps will be a Level-1

SDS product that contains a single, flux-calibrated, averaged spectrum for each spectrometer detector, $I_i(\nu)$. The spectral modification creation block is shown in Figure 3.6.

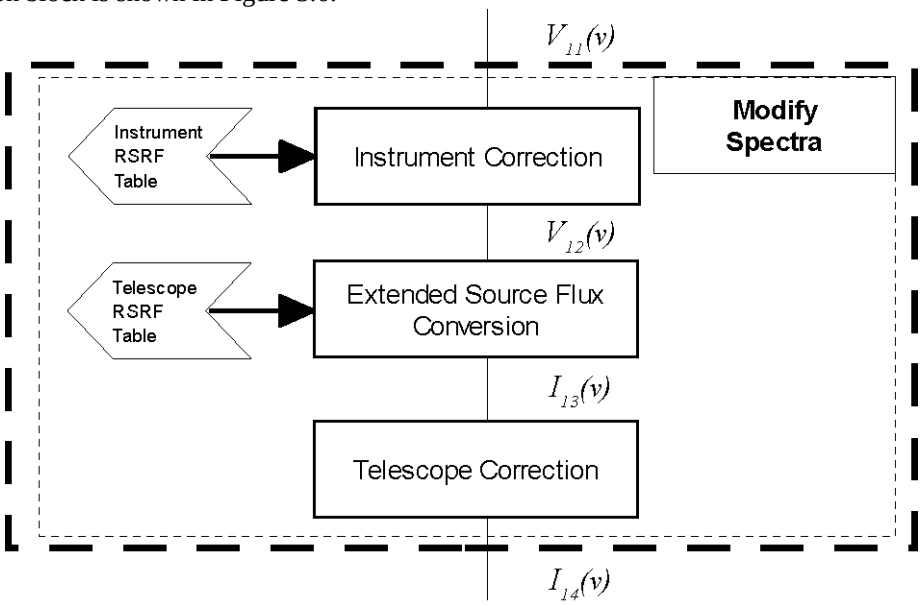

Figure 3.6: Spectral modification block of the SPIRE Spectrometer pipeline.

3.5.1 Spectrometer Instrument Correction

The equation for the total intensity of the radiation incident upon the spectrometer detectors shows that, in addition to radiation from the astronomical source, the detectors record a modulated signal from the Herschel Telescope, and a modulated signal arising from the emission of spectrometer instrument. The spectrum, $V_{11\text{-}n\text{-}i}(\nu)$, for each detector *i* and SMEC scan *n*, at this point in the building block pipeline may therefore be expressed as in Equation 3.41:

$$V_{11-n-i}(\nu) = V_{11-Source-n-i}(\nu) + V_{11-Telescope-n-i}(\nu) + V_{11-Instrument-n-i}(\nu). \quad (3.41)$$

This processing module removes from each of the measured spectra for the contribution from the SPIRE instrument. The contribution due to the SPIRE instrument, for each SMEC scan of the building block *n*, is first characterized as the product of a blackbody function at the mean recorded SCAL temperature for that scan, T_{SCAL-i}, and the Instrument RSRF, $RSRF_{Instrument\text{-}i}(\nu)$, for that detector:

$$V_{InstrumentCorrection-i}(\nu) = B(\overline{T_{SCAL-i}}, \nu) RSRF_{Instrument-i}(\nu) \quad (3.42)$$

where $B(T, \nu)$ is the Planck function,

$$B(T,\nu) = \frac{2h\nu^3}{c^2} \frac{1}{e^{h\nu/kT} - 1} \quad (3.43)$$

and

$$\begin{aligned} h &= 6.62606896 \times 10^{-34}\ [\mathrm{J\,s}], \\ k &= 1.3806505 \times 10^{-23}\ [\mathrm{J/K}], \\ c &= 2.99792458 \times 10^{8}\ [\mathrm{m/s}]. \end{aligned} \quad (3.44)$$

$$V_{12-n-i}(\nu) = V_{11-n-i}(\nu) - V_{InstrumentCorrection-n-i}(\nu) = V_{11-Source-n-i}(\nu) + V_{11-Telescope-n-i}(\nu). \quad (3.45)$$

In order to avoid any potential systematic errors, there are separate calibrated Instrument RSRF curves for each detector for each SMEC scan direction.. Thus, the operations described in Equation 3.41-Equation 3.45 should be taken as to apply independently to the spectra from the forward and reverse scans of the SPIRE mechanism. In addition, there are separate

calibrated Instrument RSRF curves for unapodized spectra and spectra apodized with a Norton-Beer 1.5 function as well as separate curves for High, Medium, and Low spectral resolutions.

3.5.2 Extended Source Spectral Response Correction and Flux Conversion

The response of the SPIRE spectrometer detector subsystem depends on the wavelength and on the spatial extent of the incoming radiation -- the response for point-like sources differs from that for sources that fill the detector's field of view, as confirmed by in-flight observations [AD02]. This module performs two functions simultaneously: it removes from the measured spectrum of each detector in the input SDS product the relative spectral response function (RSRF) for that particular detector; and it converts the spectral intensities from quantities with units of Volts/GHz to brightness quantities with units of W/m^2/Hz/sr. At this stage, since the morphology of the astronomical source is unknown, the extended source correction is applied. The correction that is to be applied is given in Equation 3.46 below:

$$I_{13-i}(\nu) = \frac{V_{12-i}(\nu)}{RSRF_{i-Telescope}(\nu)} = \frac{V_{12-Source-i}(\nu)}{RSRF_{i-Telescope}(\nu)} + \frac{V_{12-Telescope-i}(\nu)}{RSRF_{i-Telescope}(\nu)}, \text{ and} \tag{3.46}$$

$$\partial I_{13-i}(\nu) = \frac{\partial V_{12-i}(\nu)}{RSRF_{i-Telescope}(\nu)}. \tag{3.47}$$

The extended source RSRF correction and flux conversion curves, $RSRF_{i\text{-}Telescope}(\nu)$, are derived from a combination of the multiple calibration observations of the Herschel telescope and a thermal model of the Herschel telescope's primary and secondary mirrors.

Note: The calibration file applied in this step contains separate curves for each detector for each of the following cases: SMEC scan direction; unapodized or apodized with a Norton-Beer 1.5 function; High, Medium, and Low spectral resolution. In addition, because the of the presence of the SPIRE BSM in the optical chain, separate calibration curves are used for each SPIRE BSM position for spectral mapping observations.

3.5.3 Herschel Telescope Correction

This processing module applies a correction for the contribution from the Herschel telescope. As a reminder, the measured spectra at this point in the processing pipeline $I_{13\text{-}i}(\nu)$, for each detector *i*, may be expressed as in Equation 3.48:

$$I_{13-i}(\nu) = I_{13-Source-i}(\nu) + I_{13-Telescope-i}(\nu). \tag{3.48}$$

The method employed to correct for the Herschel Telescope is to subtract from the measured spectrum for each detector, $I_{13\text{-}i}(\nu)$, a model of the Telescope spectrum, $I_{TelescopeModel\text{-}i}(\nu)$ given in Equation 3.49:

$$I_{TelescopeModel-i}(\nu) = (1-\varepsilon_{tel}(\nu))\varepsilon_{tel}(\nu)B(\overline{T_{M1}},\nu) + \varepsilon_{tel}(\nu)B(\overline{T_{M2}},\nu), \tag{3.49}$$

where $\overline{T_{M1}}$ and $\overline{T_{M2}}$ represent the mean of the mean temperatures of the Herschel telescope's nine M1 and three M2 thermometers over the course of the observation building block, B(T, ν) is as in Equations 3.43 and 3.44 above, and $\varepsilon_{Tel}(\nu)$ refers to the emissivity of the Herschel telescope mirrors M1 and M2 (Equation 3.50 [RD06]):

$$\varepsilon_{tel}(\lambda) = 0.0336\lambda^{-0.5} + 0.273\lambda^{-1} \tag{3.50}$$

where λ is wavelength in microns.

The resultant spectra are given by Equation 3.51:

$$\begin{aligned} I_{14-i}(\nu) &= I_{13-i}(\nu) - I_{TelescopeModel-i}(\nu) \\ &= I_{13-Source-i}(\nu) + I_{13-Telescope-i}(\nu) - I_{TelescopeModel-i}(\nu). \\ &= I_{13-Source-i}(\nu) \end{aligned} \tag{3.51}$$

The output of this processing step will be a Level-1 Spectrometer Detector Spectrum (SDS) product.

4. LEVEL-2 SPECTRAL PRODUCTS

The final phase of the SPIRE spectrometer pipelines involves operations that modify the Level-1 spectrometer detector spectra produced by the building block pipeline to create a set of Level-2 spectral products. The format and the contents of the Level-2 spectral products depend on the observation: a point source spectrum product that contains the spectra for the central detector in each spectrometer array is produced for single pointing sparse sampling observations; a hyperspectral cube that contains two regularly spaced spatial dimensions and one spectral dimension per pixel is produced for all raster and jiggle mapping observations.

4.1 Single Pointing Sparse Sampling Observations

4.1.1 Spectral Averaging

This module computes, on a frequency-by-frequency (ν_k) basis for each spectrometer detector, i, the average of the spectral intensities across all scans, n (see Equation 4.1).

$$\overline{I_{15-i}(\nu_k)} = \frac{1}{N_{Scans}} \sum_{n=1}^{N_{Scans}} I_{n-14-i}(\nu_k)\,. \tag{4.1}$$

In addition, this module computes, on a frequency-by-frequency basis for each spectrometer detector, the uncertainty in the spectral average. The uncertainty is calculated as the standard error of the mean of the spectral components as in Equation 4.2.

$$\partial I_{15-i}(\nu_k) = \sqrt{\frac{\frac{1}{N_{Scans}-1}\sum_{n=1}^{N_{Scans}}\left(I_{n-14-i}(\nu_k) - \overline{I_{n-14-i}(\nu_k)}\right)^2}{N_{Scans}}} \tag{4.2}$$

Directional dependence. The spectral averaging processing module will provide a mechanism whereby its output product will contain two spectra per detector. One of the output spectra will contain the average computed from just the forwards scans, the other will be the average of the reverse scans. The uncertainties and the number of outliers will likewise be computed from the forward and reverse scan separately.

Regardless of whether the directionally dependent output option is chosen, the processing module will inspect, on a detector-by-detector basis, the average forward and reverse spectra for differences and report any significant differences via Quality Control.

4.1.2 Point Source Spectral Response Correction and Flux Conversion

The purpose of this processing step is essentially the same as the relative response correction and flux conversion step in the building block pipeline (see Section 3.5.2). A separate and distinct correction for point source observations is required as the correction applied in the building block pipeline is appropriate for uniform, extended sources [AD02]. In effect, this step applies the inverse of the extended source RSRF and then divides the input spectra by a frequency-dependent RSRF applicable to point-like astronomical sources:

$$I_{16-i}(\nu) = I_{15-i}(\nu) \times RSRF_{Telescope-i}(\nu) \times \frac{f_{Point-i}(\nu)}{RSRF_{Point-i}(\nu)}\text{, and} \tag{4.3}$$

$$\partial I_{16-i}(\nu) = \partial I_{15-i}(\nu) \times RSRF_{Telescope-i}(\nu) \times \frac{f_{Point-i}(\nu)}{RSRF_{Point-i}(\nu)}\,. \tag{4.4}$$

The conversion curves, $f_{i\text{-}Point}(\nu)/RSRF_{i\text{-}Point}(\nu)$, are derived from the results of an observation of Uranus and a model of its brightness [RD07]. The final Level-2 point source spectrum product contains spectra for only the central detectors of each array.

Note: The calibration file applied in this step contains separate curves for each detector for each of the following cases: unapodized or apodized with a Norton-Beer 1.5 function; and High, Medium, and Low spectral resolution.

4.2 Mapping Observations

4.2.1 Spatial Regridding

The Level-1 spectral products created by the spectrometer building block pipeline contain one spectrum per detector. The spatial distribution of the spectra in the astronomical region of interest is determined by the hexagonally closed packed format of the detector arrays (Figure 4.1).

The spatial regridding step is applied to the set of Level-1 SDS products for all SPIRE spectrometer mapping observations – all raster observations and/or those performed at intermediate or full spatial sampling (Figure 4.2, Figure 4.3). This step interpolates the Level-1 spectra onto a hyperspectral data cube that is equidistantly sampled in the two spatial dimensions but leaves the equidistant grid along the spectral dimension unchanged.

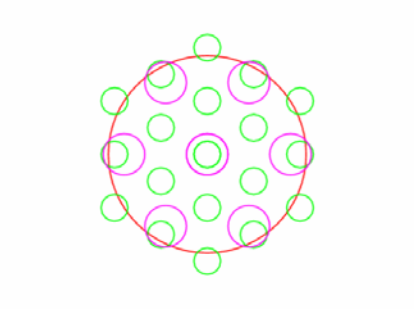

Figure 4.1: Sparse spatial sampling mode. [AD02]

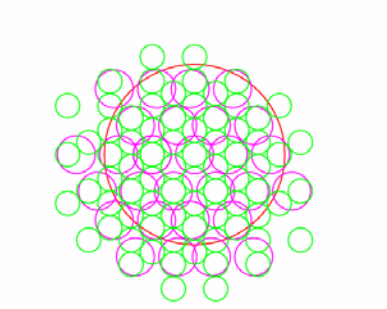

Figure 4.2: Intermediate spatial sampling mode. [AD02]

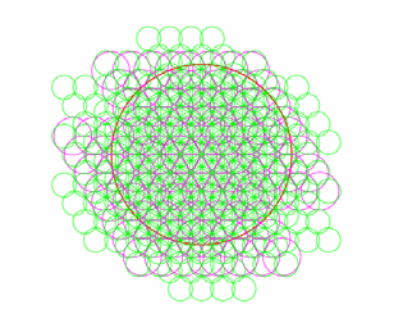

Figure 4.3: Full spatial sampling mode. [AD02]

The process of regridding the Level-1 spectral data involves first the creation of a suitable target grid in coordinates of Right Ascension and Declination. The pixel size within this target grid depends on the spatial sampling of the observation and is given in Table 2.2. The World Coordinate System (WCS) for a given observation is calculated as follows: The minimum and maximum values of Right Ascension and Declination of the individual spectra are determined. The ranges in Right Ascension and Declination are calculated as the difference between the maximum and minimum values. The preliminary number of pixels in each direction is calculated by dividing the Right Ascension and Declination ranges by the specified pixel sizes. The reference world coordinates of the WCS are set at the centre pixel of the WCS to the average of the minimum and maximum Right Ascension and Declination values. The units of Right Ascension, Declination, and the frequency are propagated without changes. The projection type is set to RA--TAN and DEC-TAN. The Right Ascension and Declination system is set to "Equatorial". This procedure can lead to additional rows and columns which are not covered by observations. The final number of pixels is set as follows: Determine the range of pixel coordinate values of the current WCS. Shift the reference pixel coordinates in each direction by the amount by which the lowest pixel coordinate value differs from 0.5. Set the number of pixels in each direction to be equal to the minimum number of pixels required to cover the observed spectra.

Finally, the spectrum in each pixel of the target spatial grid is determined with the Naive projection algorithm – the same algorithm as is used for scanning observations with the SPIRE photometer. The Naive projection algorithm computes the flux and uncertainty in a given map pixel as the mean and standard error of the mean of all samples within that pixel, respectively. The map pixel is set to Not-A-Number if no samples were taken within the pixel. Naive projection iterates though all spectral bins and applies the naive mapping for each slice independently. The Naive projection algorithm also provides as output a coverage map – a map where each pixel contains the number of samples that were used to compute the flux average and uncertainty.

An alternate algorithm that takes into account spectral uncertainties is currently under development and evaluation:

HIFI Gridding. The HIFI instrument team has implemented an algorithm to grid spectral data that were taken in the On-The-Fly observing mode onto a regular spatial grid. The software implements an algorithm that is based on work in image processing. This can also be applied to SPIRE data by iterating though all spectral bins and applying the algorithm for each slice independently.

5. BRIGHT MODE PROCESSING

The pipelines for SPIRE Spectrometer observations made using bright source mode are similar to the nominal mode pipelines, which were described in §3 and §4. This section describes the differences between the two sets of pipelines as well as the processing modules that are specific to the bright mode pipelines.

5.1 Base Units

The main difference between the nominal mode and bright mode SPIRE Spectrometer pipelines is in the base units used during processing. In the nominal mode pipelines described in §3 and §4, the base signal units are Volts or Volts/GHz until such time as the extended source flux conversion is applied (Section 3.5.2). The base units in the bright mode pipeline are Kelvin (Section 5.2.1) or Kelvin/GHz and remain so until the extended source flux conversion is applied. The reason for this difference is that the bright source mode uses different bolometer bias settings (voltage and phase). These differences affect the responsivity of the detectors and mean that a different calibration to astronomical units would be required for bright mode. In order to make use of the same high signal-to-noise calibration observations as used for nominal mode, the effect of changing the detector bias is accounted for at the beginning of the pipeline using a bolometer model to convert voltage to bolometer temperature.

5.2 Modify Timelines

The processing modules described in the following sections are applied to the timelines for each spectrometer detector. Each of the processing steps contained in this processing block (see Figure 5.1) accepts a Level-0.5 SDT product as input and delivers an SDT product as output.

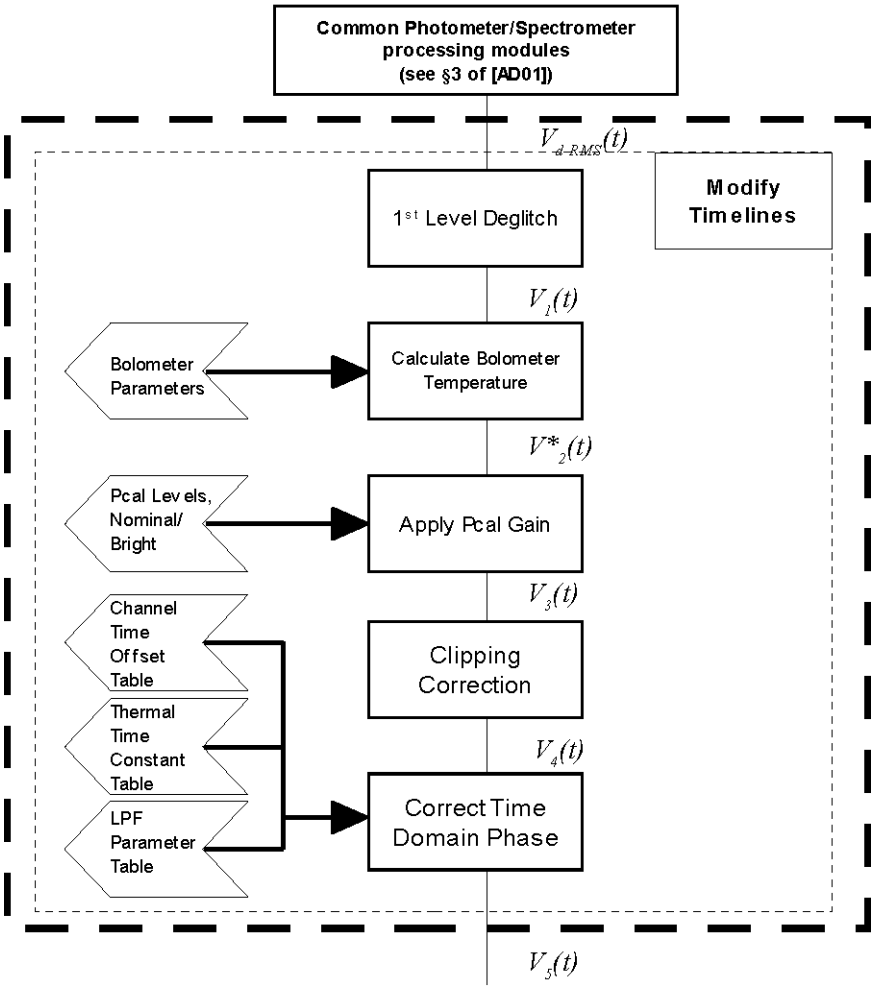

Figure 5.1: Timeline modification block of the bright mode SPIRE Spectrometer pipeline.

5.2.1 Calculating Bolometer Temperature and Optical Power

This module uses a model of the bolometers [RD08] to compute the bolometer temperature and optical power ($T_{2\text{-}i}(t) \equiv V_{2\text{-}i}(t)$) from the deglitched bolometer voltage timelines, $V_{i\text{-}i}(t)$.

The first step of the calculate optical power module computes, for each bolometer *i*, a resistance timeline, $R_{2\text{-}i}(t)$, from the incoming voltage timelines, $V_{2\text{-}i}(t)$, incoming bias voltages, $V_{Bias\text{-}i}$, and load resistance, $R_{L\text{-}i}$, as in Equation 5.1.

$$R_{2-i}(t) = \frac{V_{Bias-i}}{\left(V_{Bias-i} - V_{1-i}(t)\right) \Big/ R_{L-i}} - R_{L-i} \tag{5.1}$$

Next, resistance timelines are then converted to bolometer temperature as in Equation 5.2.

$$T_{2-i}(t) \equiv V_{2-i}(t) = \frac{\Delta}{\left[\ln\left(\frac{R_{2-i}(t)}{R_{0-i}}\right)\right]^2} \tag{5.2}$$

The module can also be used to calculate the optical power incident on the bolometers, but this is not used in the pipeline.

5.2.2 Apply PCAL Gain

This module applies an empirically derived gain correction for bright source mode observations, by comparing the PCAL level separation in the observation itself with the mean value for Nominal Mode. The PCAL level separation must be supplied in the output format of the PCal task (see Section 2.1 of [AD06] for a description of PCAL flash processing).

The PCAL Gain module computes, for each spectrometer detector *i*, the ratio of a measured PCAL flash level separation ($PCal_{\text{Bright-}i}$) to the mean PCAL flash separation measured on Dark Sky in Nominal Mode ($PCal_{\text{Nominal-}i}$) – see Equation 5.3. The module applies this ratio as a gain term to the incoming detector timelines– see Equation 5.4.

$$PCalGain_i = \frac{PCal_{\text{Nominal}-i}}{PCal_{\text{Bright}-i}} \tag{5.3}$$

$$V_{3-i}(t) = V_{2-i}(t) \times PCalGain_i \tag{5.4}$$

5.3 Modify Spectra

The pipeline modules that follow in this section describe the operations that will be performed on the Level-0.5 SDS products that were created by the Fourier Transform task (Section 3.4.1). The end result of these spectral modifying processing steps will be a Level-1 SDS product that contains a single, flux-calibrated, averaged spectrum for each spectrometer detector, $I_i(\nu)$. The spectral modification creation block is shown in Figure 5.2.

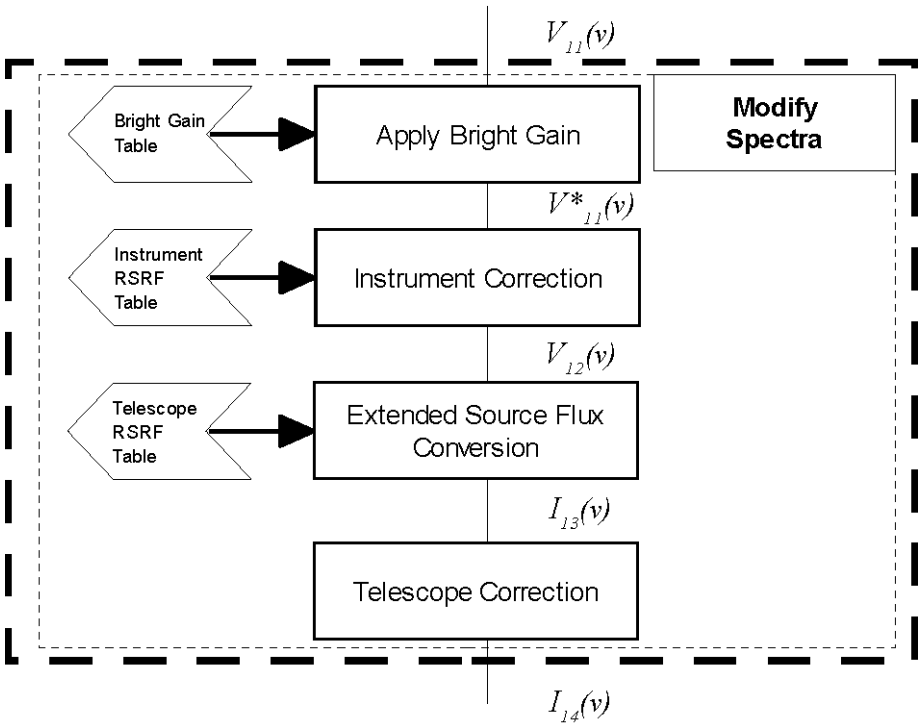

Figure 5.2: Spectral modification block of the bright mode SPIRE Spectrometer pipeline.

5.3.1 Apply Bright Mode Gain

The Bright Mode Gain module computes and then applies a frequency-dependent gain factor for observations which have been made using the bright source mode (the PCAL gain factor described in Section 5.2.2 is a single number for all frequencies in each band). This module applies to the incoming spectra of each detector *i* a linear gain correction factor defined by calibrated intercept and gradient terms (b_i and m_i) as in Equation 5.5.

$$V^*_{11-i}(\nu) = V_{11-i}(\nu)\left(m_i\nu + b_i\right) \tag{5.5}$$

Appendix A.1. First Level Deglitching Description

1. **Glitch Identification.** Glitch signatures are detected by performing a local regularity analysis (Holderian analysis) over the wavelet transform modulus maxima lines (WTMML) of the signal.

   Let H be the Holder exponent, s the scale of decomposition, $X_i(s)$ the time (or OPD) domain coordinate of the maxima line for the scale s, then when the scale s goes to zero the corresponding wavelet coefficient, $W(X_i(s),s)$, is given by:

   $$W(X_i(s), s) \le Cs^H \quad \text{(A1.1)}$$

   where C is a real constant.

   The scale of decomposition, s, may be expressed over a logarithmic scale as:

   $$s = 2^o 2^{v/n_V} \quad \text{(A1.2)}$$

   where positive integers o, n_V, and v (with $v < n_V$) are respectively called octave, number of voices, and voice of the decomposition 1, respectively.

   On each maxima line, the regularity degree of the signal is estimated by computing the slope of the linear regression over the set of points ($\log_2(|W|)$, $\log_2(s)$) over the range of scales [scaleMin, scaleMax]. If the relation is linear; i.e. if the square of its correlation coefficient C is greater than the threshold coefficient, correlationThreshold; then the Holder exponent H can be estimated by the measure of the slope of the relation. Glitches are detected as they are similar to Dirac-like signatures and show a Holder exponent (i.e. regularity degree) close to -1, in a range defined by two input parameters, H_{min}, H_{max}, centered about -1.

   Noise can generate false detections (it can be shown that the Holder exponent of a Gaussian noise has a value (in mean) of 0.5). In order to minimize the likelihood of these false positives, constraints are applied to the wavelet coefficients. By considering a Gaussian noise of standard deviation s, it can be shown that at the lowest scale of decomposition, the following threshold:

   $$|W| \le \sigma\sqrt{2\ln N} \quad \text{(A1.3)}$$

   where N is the size of the signal.

   The noise standard deviation s on the signal can be estimated using the Donoho estimator; at the lowest scale, s = 0.6745 × med |W|. For each maxima line, if the value of the wavelet coefficient for the first scale value is greater than the previous threshold an estimate is made of the regularity degree.

2. **Glitch Reconstruction.** Each sample that is identified as a glitch by the preceding step is replaced, along with its nearest neighbours (see below), by way of a sixth order polynomial fit applied to the nearest eight points surrounding the samples to be replaced.

The parameters that follow are optional and have been optimized for the SPIRE spectrometer detectors. SPIRE PFM1 data that, by visual inspection, contained 29 glitches was used as a basis for this optimization.

- **scaleMin**, **scaleMax**: The scale range used for the linear regression. Optimal values are scaleMin = 1 and scaleMax = 8.
- **scaleInterval**: The scale range used for the linear regression. Optimal value is 5.
- **H_{min}, H_{max}**: The Holder exponent range used to select a glitch. Optimal values are H_{min} = -1.4 and H_{max} = -0.6.
- **correlationThreshold**: The square threshold correlation that defines linear behaviour. The optimal value is correlationThreshold= 0.85.
- **Number of points in reconstruction, n_{Before}, n_{After}**: The number of points to include in the glitch reconstruction in the neighbourhood of the detected glitch. Optimal values are: n_{Before} = 2 and n_{After} = 3.

Appendix A.2. RADIATION INCIDENT ON THE SPIRE SPECTROMETER DETECTORS

The radiation path through the SPIRE spectrometer is illustrated for one case in Figure A2.1.

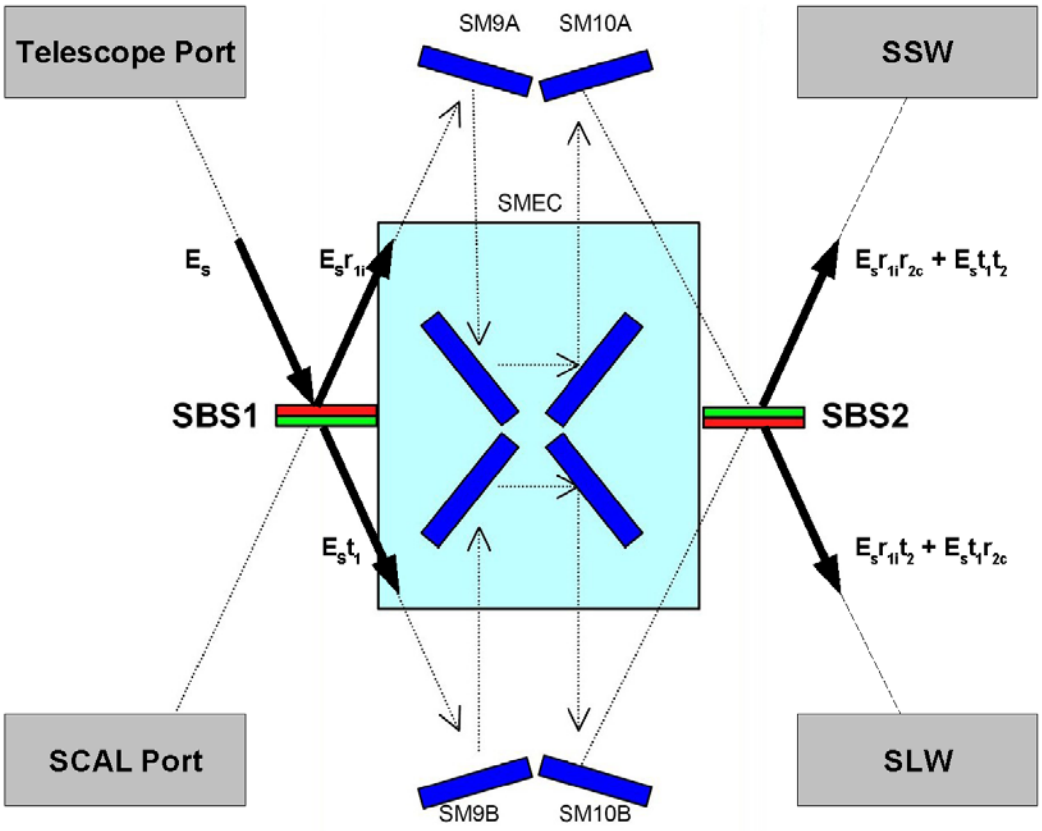

Figure A2.1:

As shown in Figure A2.1, the first beamsplitter (SBS1) divides the incoming electric field (E_S) into two components ($E_S r_{1c}$ and $E_S t_1$). These two components pass through the interferometer and then are split further at the second beamsplitter (SBS2). The upper beam from Figure A2.1 then passes to the SSW detectors while the lower beam passes to the SLW detectors. The electric fields incident on the SSW and SLW detectors are given by the following equations:

$$E_{S-SSW}(x,\nu) = E_{s_0}(\nu)\left[r_{1_i} r_{2_c} e^{-i2\pi(\nu x_1 - ft)} + t_1 t_2 e^{-i2\pi(\nu x_2 - ft)}\right] \quad \text{(A2.1)}$$

$$E_{S-SLW}(x,\nu) = E_{s_0}(\nu)\left[r_{1_i} t_2 e^{-i2\pi(\nu x_1 - ft)} + t_1 r_{2_c} e^{-i2\pi(\nu x_2 - ft)}\right] \quad \text{(A2.2)}$$

At the detectors, the intensity recorded is the time-average of the square of the incident electric field. Using the SSW detectors for illustration, the measured intensity for radiation from an astronomical source at the detectors is given by the following:

$$I_S(x,\nu) = \frac{c\varepsilon_0}{2} E_S^*(x,\nu) E_S(x,\nu) \quad \text{(A2.3)}$$

where:

$$\begin{aligned} E_S^*(x,\nu)E_S(x,\nu) &= E_{S_0}^*(\nu)\left[r_{1_i} r_{2_c} e^{-i2\pi(\nu x_1 - ft)} + t_1 t_2 e^{-i2\pi(\nu x_2 - ft)}\right] \times E_{S_0}(\nu)\left[r_{1_i} r_{2_c} e^{-i2\pi(\nu x_1 - ft)} + t_1 t_2 e^{-i2\pi(\nu x_2 - ft)}\right] \\ &= E_{S_0}^2(\nu)\left[\left(r_{1_i} r_{2_c}\right)^2 + \left(t_1 t_2\right)^2 + 2 r_{1_i} r_{2_c} t_1 t_2 \cos(2\pi\nu(x_1 - x_2))\right] \end{aligned} \quad \text{(A2.4)}$$

Combining the above results in the following equations for the measured intensity at the SSW and SLW detectors for radiation from an astronomical source:

$$
\begin{aligned}
I_{SSW}(x) &= \int_0^\infty I_{SSW}(x,\nu)d\nu \\
&= \int_0^\infty E_0^2(\nu)\left[\left(r_{1_i}r_{2_c}\right)^2 + \left(t_1t_2\right)^2 + 2r_{1_i}r_{2_c}t_1t_2\cos(2\pi\nu x)\right]d\nu \\
&= I_{SSW}(0)\left[\left(r_{1_i}r_{2_c}\right)^2 + \left(t_1t_2\right)^2\right] + 2\int_0^\infty \left[r_{1_i}r_{2_c}t_1t_2\right]B(\nu)\cos(2\pi\nu x)d\nu \\
&= I_{SSW-Offset} + I_{SSW-Modulated}(x)
\end{aligned}
\tag{A2.5}
$$

$$
\begin{aligned}
I_{SLW}(x) &= \int_0^\infty I_{SLW}(x,\nu)d\nu \\
&= \int_0^\infty E_0^2(\nu)\left[\left(r_{1_i}t_2\right)^2 + \left(t_1r_{2_c}\right)^2 + 2r_{1_i}r_{2_c}t_1t_2\cos(2\pi\nu x)\right]d\nu \\
&= I_{SLW}(0)\left[\left(r_{1_i}t_2\right)^2 + \left(t_1r_{2_c}\right)^2\right] + 2\int_0^\infty \left[r_{1_i}r_{2_c}t_1t_2\right]B(\nu)\cos(2\pi\nu x)d\nu \\
&= I_{SLW-Offset} + I_{SLW-Modulated}(x)
\end{aligned}
\tag{A2.6}
$$

In addition to the astronomical source, radiation from the Herschel telescope and the three components of SCAL (SCAL2, SCAL4, and SCAL) is incident on the SPIRE spectrometer detectors. For the telescope radiation, its path through the SPIRE spectrometer is the same as that for the astronomical source. The path for the SCAL emitters is slightly different (see Figure A2.1). The equations for the radiation incident on the SSW and SLW detectors are given by the following:

$$
\begin{aligned}
I_{SSW}(x) &= \int_0^\infty I_{SSW}(x,\nu)d\nu \\
&= \int_0^\infty E_0^2(\nu)\left[\left(r_{1_c}t_2\right)^2 + \left(t_1r_{2_c}\right)^2 + 2r_{1_c}r_{2_c}t_1t_2\cos(2\pi\nu x)\right]d\nu \\
&= I_{SSW}(0)\left[\left(r_{1_c}r_{2_c}\right)^2 + \left(t_1t_2\right)^2\right] + 2\int_0^\infty \left[r_{1_c}r_{2_c}t_1t_2\right]B(\nu)\cos(2\pi\nu x)d\nu \\
&= I_{SSW-Offset} + I_{SSW-Modulated}(x)
\end{aligned}
\tag{A2.7}
$$

$$
\begin{aligned}
I_{SLW}(x) &= \int_0^\infty I_{SLW}(x,\nu)d\nu \\
&= \int_0^\infty E_0^2(\nu)\left[\left(r_{1_c}t_2\right)^2 + \left(t_1r_{2_i}\right)^2 + 2r_{1_c}r_{2_i}t_1t_2\cos(2\pi\nu x)\right]d\nu \\
&= I_{SLW}(0)\left[\left(r_{1_c}t_2\right)^2 + \left(t_1r_{2_i}\right)^2\right] + 2\int_0^\infty \left[r_{1_c}r_{2_i}t_1t_2\right]B(\nu)\cos(2\pi\nu x)d\nu \\
&= I_{SLW-Offset} + I_{SLW-Modulated}(x)
\end{aligned}
\tag{A2.8}
$$

Taken together, the overall intensity of the radiation measured by the SPIRE spectrometer detectors is given by the following:

$$
I_{TOTAL}(x) = I_{Source}(x) + I_{Telescope}(x) + I_{Beamsplitter}(x) + I_{SCAL}(x) + I_{SCAL2}(x) + I_{SCAL4}(x) \tag{A2.9}
$$

1. SSW Detectors.

$$I_{SSW}(x) = \left(I_{Source}(0) + I_{Telescope}(0) + I_{Beamsplitter}(0)\right)\left[\left(r_{1_i} r_{2_c}\right)^2 + \left(t_1 t_2\right)^2\right]$$
$$+ \left(I_{SCAL}(0) + I_{SCAL2}(0) + I_{SCAL4}(0)\right)\left[\left(r_{1_c} t_2\right)^2 + \left(t_1 r_{2_c}\right)^2\right] + 2\int_0^\infty \left[r_{1_i} r_{2_c} t_1 t_2\right] B_{Source}(\nu)\cos(2\pi\nu x)d\nu$$
$$+ 2\int_0^\infty \left[r_{1_i} r_{2_c} t_1 t_2\right] B_{Telescope}(\nu)\cos(2\pi\nu x)d\nu + 2\int_0^\infty \left[r_{1_i} r_{2_c} t_1 t_2\right] B_{Beamsplitter}(\nu)\cos(2\pi\nu x)d\nu \quad \text{(A2.10)}$$
$$- 2\int_0^\infty \left[r_{1_c} r_{2_c} t_1 t_2\right] B_{SCAL}(\nu)\cos(2\pi\nu x)d\nu - 2\int_0^\infty \left[r_{1_c} r_{2_c} t_1 t_2\right] B_{SCAL2}(\nu)\cos(2\pi\nu x)d\nu$$
$$- 2\int_0^\infty \left[r_{1_c} r_{2_c} t_1 t_2\right] B_{SCAL4}(\nu)\cos(2\pi\nu x)d\nu$$

2. SLW Detectors.

$$I_{SLW}(x) = \left(I_{Source}(0) + I_{Telescope}(0) + I_{Beamsplitter}(0)\right)\left[\left(r_{1_i} t_2\right)^2 + \left(t_1 r_{2_i}\right)^2\right]$$
$$+ \left(I_{SCAL}(0) + I_{SCAL2}(0) + I_{SCAL4}(0)\right)\left[\left(r_{1_c} r_{2_i}\right)^2 + \left(t_1 t_2\right)^2\right] + 2\int_0^\infty \left[r_{1_i} r_{2_i} t_1 t_2\right] B_{Source}(\nu)\cos(2\pi\nu x)d\nu$$
$$+ 2\int_0^\infty \left[r_{1_i} r_{2_i} t_1 t_2\right] B_{Telescope}(\nu)\cos(2\pi\nu x)d\sigma + 2\int_0^\infty \left[r_{1_i} r_{2_i} t_1 t_2\right] B_{Beamsplitter}(\nu)\cos(2\pi\nu x)d\nu \quad \text{(A2.11)}$$
$$- 2\int_0^\infty \left[r_{1_c} r_{2_i} t_1 t_2\right] B_{SCAL}(\nu)\cos(2\pi\nu x)d\sigma - 2\int_0^\infty \left[r_{1_c} r_{2_i} t_1 t_2\right] B_{SCAL2}(\nu)\cos(2\pi\nu x)d\nu$$
$$- 2\int_0^\infty \left[r_{1_c} r_{2_i} t_1 t_2\right] B_{SCAL4}(\nu)\cos(2\pi\nu x)d\nu$$

Appendix A.3. DOUBLE-SIDED AND SINGLE-SIDED INTERFEROGRAMS

The terms double-sided and single-sided as used in this document describe the two types of interferograms that can be measured with a Fourier Transform Spectrometer.

Double-sided Interferograms

Double-sided interferograms are defined as those interferograms or that portion of measured interferogram where the sample positions are symmetric about the position of zero path difference (ZPD). That is, a double-sided interferogram is one that contains an equal number of samples before and after the ZPD sample 2[1]. An envelope of a double-sided interferogram is shown in Figure A3.1.

[1] Some implementations of the Fourier Transform may require an even number of points ($N_{TOTAL} \equiv$ Even). In this case, the RHS of the double-sided interferogram will contain an extra point.

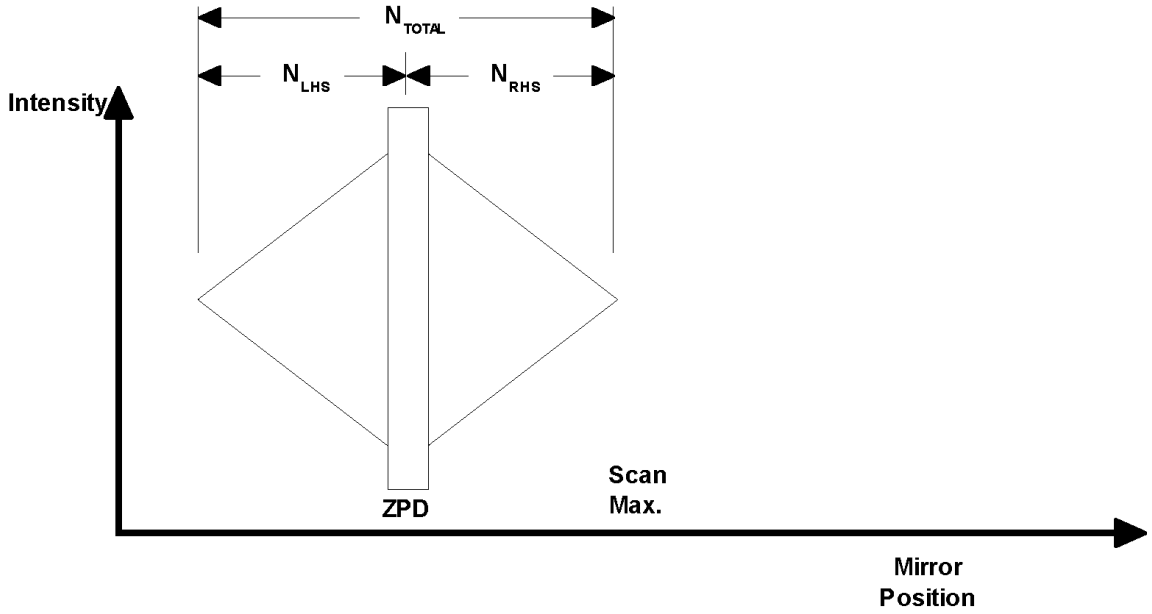

Figure A3.1: Envelope of a double-sided interferogram

Single-sided interferograms

Single-sided interferograms are defined as those interferograms that contain more samples on one side of ZPD than the other. An envelope of a single-sided interferogram is shown in Figure A3.2.

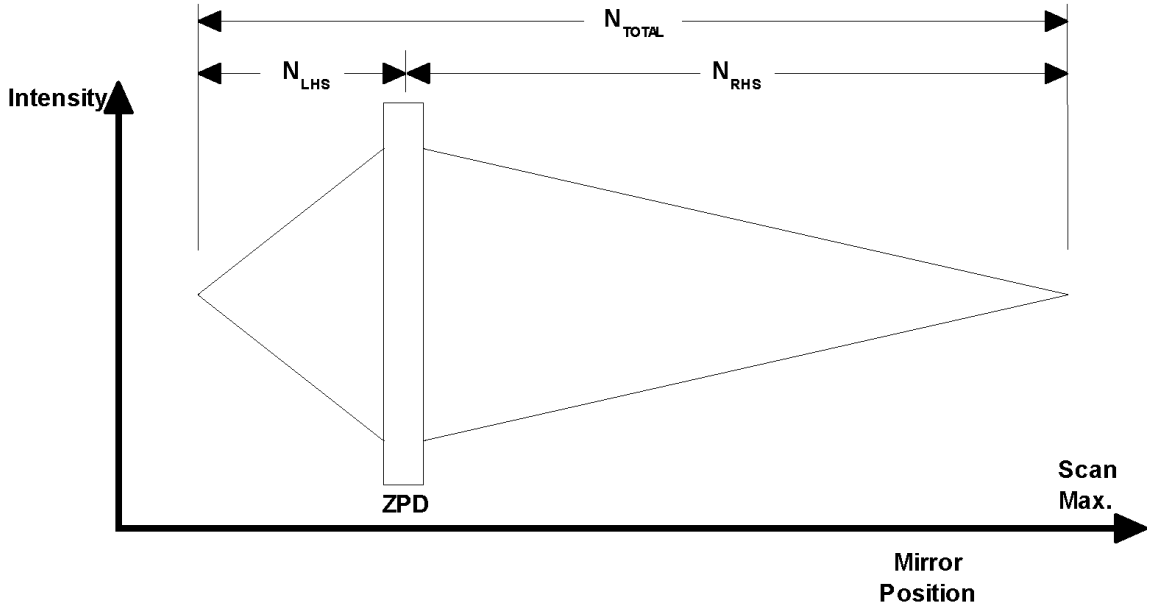

Figure A3.2: Envelope of a Single-sided interferogram

Appendix A.4. OUTLIER REJECTION FOR SMALL SAMPLE SIZES

Flagging outliers via Sigma Clipping. Sigma Clipping flags a sample within a distribution as an outlier if the absolute difference between its value and the average m is larger than d times the standard deviation s. Typically, d is set to 3 which, in the case of an infinitely large sample, sets the probability to identify an outlier in a randomly distributed sample to less than 1% (0.27% to be specific).

$$x \text{ is an outlier iff } \frac{x-m}{s} > d$$

Sigma Clipping for very small sample sizes. In most real-life situations, the average m and standard deviation s of a sample are not known a priori. In those cases, the elements of the sample can be used to estimate the average m and standard deviation s. The arithmetic mean and the standard deviation of the values in the sample provide a good estimate of m and s if the sample size is large. This note focuses on the case of small sample sizes (N<20) where one cannot, therefore, assume that the estimates of the average and standard deviation from the sample themselves are good.

A simple simulation shows that it is impossible for sample sizes up to N=10 to have a normalized deviation of d>3.0 when deriving the arithmetic mean and the standard deviation from the measurements themselves (see Figure A4.1). The most extreme case – an almost homogeneous sample with one arbitrarily large outlier – is characterized by a value of d=2.846 for N=10). Put differently: Straightforward 3-sigma clipping, as defined above, cannot flag any outliers in samples of 10 or fewer elements. This is due to an effect called "swamping". In a small sample, even a single strong outlier will affect the estimate of both, the average and the standard deviation, rendering sigma clipping very insensitive. The swamping effect can be partially remedied by using the median to determine the average value of the sample. Note that this will not fully resolve the problem for the increased standard deviation which is more strongly affected by outliers than the average, since the residuals add in quadrature.

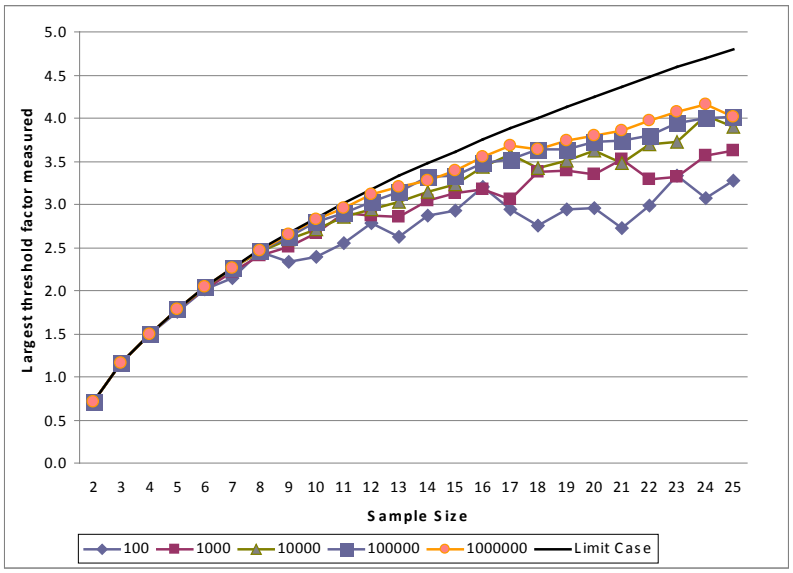

Figure A4.1: The largest, simulated normalized deviation for small sample sizes between 2 and 25 for 100 through 1,000,000 trials and the most extreme case of an almost homogeneous sample.

Indeed, for N=2, it can be shown that the normalized deviation, i.e. the difference between the value of an element and the average divided by the standard deviation, is equal to the square root of ½, independent of the values in the sample. In this case, sigma-clipping should never be employed to identify outliers since it will either flag no or all samples as outliers.

Sigma Clipping with a threshold that varies as a function of sample size. In order to define an outlier rejection algorithm that performs well when applied to small sample sizes, it seems preferable to vary the applicable threshold factor with the sample size. For instance, the threshold factor can be set in such a way that less than x% outliers are flagged in randomly distributed data. The remainder of this note reports those threshold factors for sigma clipping, which flag 0.1% or 0.5% outliers in a normally distributed sample of N elements (N between 2 and 25) in a computer simulation with 100,000 trials (see Figure A4.2 and Table A4.1).

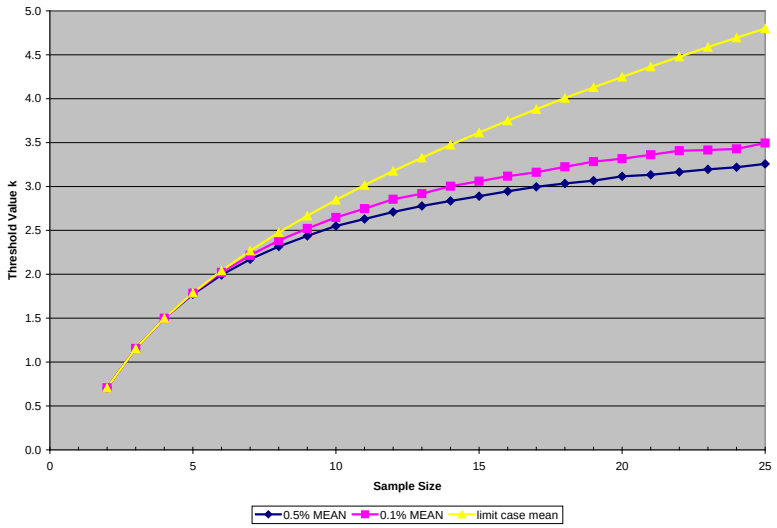

Figure A4.2: Setting outlier rejection at the desired level (0.5% and 0.1%) for 100,000 trials determines the threshold factor for the sigma-clipping outlier rejection algorithm.

Sample size	d with 0.5% false pos.	d with 0.1% false pos.	Limit case
2	0.707	0.707	0.707
3	1.155	1.155	1.155
4	1.498	1.500	1.500
5	1.773	1.784	1.789
6	1.993	2.021	2.041
7	2.172	2.216	2.268
8	2.316	2.385	2.475
9	2.438	2.521	2.667
10	2.551	2.647	2.846
11	2.629	2.747	3.015
12	2.709	2.854	3.175
13	2.779	2.919	3.328
14	2.836	3.002	3.474
15	2.889	3.061	3.615
16	2.946	3.118	3.750
17	2.996	3.161	3.881
18	3.034	3.224	4.007
19	3.067	3.283	4.129
20	3.115	3.316	4.249
21	3.134	3.361	4.364
22	3.166	3.408	4.477
23	3.195	3.415	4.587
24	3.219	3.428	4.695
25	3.257	3.495	4.800

Table A4.1: The threshold value to flag fewer than 0.5% and 0.1% false positives in a randomly distributed sample of size 2 through 25, as determined in 100,000 trials. The limit case for an almost homogeneous distribution is also added.

Appendix A.5. SECOND LEVEL GLITCH DETECTION ALGORITHMS

The second level deglitching module offers four different methods for glitch detection. The algorithms for each method are described below.

1. **Standard deviation glitch detection.** For each detector, i, in the input Interferogram product, this glitch detection algorithm:
   a. calculates the standard deviation across scans, n, for each OPD position, x_k;
   b. calculates the mean across scans for each OPD position;
   c. then, at each OPD position, x_k, the module identifies as a glitch those samples whose value deviates from the mean by more than a threshold factor multiplied by the standard deviation at that OPD position.

   Note: This detection method requires at least 3 scans in each scan direction to function properly.

2. **Median Absolute Deviation (MAD) detection.** For each detector, i, in the input Interferogram product, this glitch detection algorithm:
   a. calculates the MAD across scans, n, for each OPD position, x_k;
   b. calculates the median across scans for each OPD position;
   c. then, at each OPD position, x_k, the module identifies as a glitch those samples whose value deviates from the median by more than a threshold factor multiplied by the MAD at that OPD position.

3. **Windowed standard deviation glitch detection.** For each detector, i, in the input Interferogram product, this glitch detection algorithm:
   a. calculates the standard deviation across scans, n, for each OPD position, x_k, (i.e. a the Standard deviation interferogram is computed);
   b. calculates the mean of the standard deviation interferogram of a window of width *w*, centred about each OPD position, x_k;
   c. calculates the standard deviation of the standard deviation interferogram of a window of width *w*, centred about each OPD position, x_k;
      Note: the mean and standard deviations computed here are invalid for position elements, x_k, for which the window extends beyond the extrema of the standard deviation interferogram. In these cases, these entries are assigned the values from the nearest valid OPD position.
   d. then, at each OPD position, x_k, the module identifies the presence of a glitch if the value of the standard deviation interferogram at that sample deviated from the windowed mean by more than a factor multiplied by the windowed standard deviation. If this threshold is exceeded then the scan that contains the sample that deviates the most from the median is removed and steps a. to d are re-evaluated.

4. **Windowed median Absolute Deviation (MAD) detection.** For each detector, i, in the input Interferogram product, this glitch detection algorithm:
   a. calculates the standard deviation across scans, n, for each OPD position, x_k, (i.e. a the Standard deviation interferogram is computed);
   b. calculates the median of the standard deviation interferogram of a window of width *w*, centred about each OPD position, x_k;
   c. calculates the MAD of the standard deviation interferogram of a window of width *w*, centred about each OPD position, x_k;
      Note: the median and MAD computed here are invalid for position elements, x_k, for which the window extends beyond the extrema of the standard deviation interferogram. In these cases, these entries are assigned the values from the nearest valid OPD position.
   d. then, at each OPD position, x_k, the module identifies the presence of a glitch if the value of the standard deviation interferogram at that sample deviated from the windowed median by more than a factor multiplied by the windowed MAD. If this threshold is exceeded then the scan that contains the sample that deviates the most from the median is removed and steps a. to d. are re-evaluated.